The Journal of Chemical Physics

RESEARCH ARTICLE | APRIL 22 2024

HCl trimer: HCl-stretch excited intramolecular and intermolecular vibrational states from 12D fully coupled quantum calculations employing contracted intra- and inter-molecular bases

Irén Simkó ; Peter M. Felker ; Zlatko Bačić

J. Chem. Phys. 160, 164304 (2024)
https://doi.org/10.1063/5.0207366

AIP Publishing

The Journal of Chemical Physics ARTICLE pubs.aip.org/aip/jcp

HCl trimer: HCl-stretch excited intramolecular and intermolecular vibrational states from 12D fully coupled quantum calculations employing contracted intra- and inter-molecular bases

Cite as: J. Chem. Phys. 160, 164304 (2024); doi: 10.1063/5.0207366
Submitted: 7 March 2024 • Accepted: 7 April 2024 •
Published Online: 22 April 2024

Irén Simkó,[1,2,a] Peter M. Felker,[3,b] and Zlatko Bačić[1,2,4,c]

AFFILIATIONS

[1] Department of Chemistry, New York University, New York, New York 10003, USA
[2] Simons Center for Computational Physical Chemistry at New York University, New York, New York 10003, USA
[3] Department of Chemistry and Biochemistry, University of California, Los Angeles, California 90095-1569, USA
[4] NYU-ECNU Center for Computational Chemistry at NYU Shanghai, 3663 Zhongshan Road North, Shanghai 200062, China

[a] **Electronic mail:** is2873@nyu.edu
[b] **Electronic mail:** felker@chem.ucla.edu
[c] **Author to whom correspondence should be addressed:** zlatko.bacic@nyu.edu

ABSTRACT

We present fully coupled, full-dimensional quantum calculations of the inter- and intra-molecular vibrational states of HCl trimer, a paradigmatic hydrogen-bonded molecular trimer. They are performed utilizing the recently developed methodology for the rigorous 12D quantum treatment of the vibrations of the noncovalently bound trimers of flexible diatomic molecules [Felker and Bačić, J. Chem. Phys. **158**, 234109 (2023)], which was previously applied to the HF trimer by us. In this work, the many-body 12D potential energy surface (PES) of $(HCl)_3$ [Mancini and Bowman, J. Phys. Chem. A **118**, 7367 (2014)] is employed. The calculations extend to the intramolecular HCl-stretch excited vibrational states of the trimer with one- and two-quanta, together with the low-energy intermolecular vibrational states in the two excited $v = 1$ intramolecular vibrational manifolds. They reveal significant coupling between the intra- and inter-molecular vibrational modes. The 12D calculations also show that the frequencies of the $v = 1$ HCl stretching states of the HCl trimer are significantly redshifted relative to those of the isolated HCl monomer. Detailed comparison is made between the results of the 12D calculations on the two-body PES, obtained by removing the three-body term from the original 2 + 3-body PES, and those computed on the 2 + 3-body PES. It demonstrates that the three-body interactions have a strong effect on the trimer binding energy as well as on its intra- and inter-molecular vibrational energy levels. Comparison with the available spectroscopic data shows that good agreement with the experiment is achieved only if the three-body interactions are included. Some low-energy vibrational states localized in a secondary minimum of the PES are characterized as well.

I. INTRODUCTION

Noncovalent, hydrogen-bonded (HB) and van der Waals (vdW) interactions are of profound significance, having a major role in shaping the structural and dynamical properties of matter on all scales, ranging from small molecular complexes and molecular clusters to liquid and solid condensed phases, as well as biomacromolecules and key biological structures, such as cellular membranes. For decades, this has made them the subject of increasingly more elaborate studies by experimentalists and theorists alike.

Noncovalently bound molecular complexes, binary and ternary in particular, have been long been the favorite target in this context. Their relatively low dimensionality and simplicity allow investigating HB and vdW interactions that bind them with the sophistication and level of detail and accuracy that would be impossible for more complex systems. The high-resolution infrared (IR), far-IR, and Raman spectra of noncovalently bound complexes encode a great

deal of information about their potential energy surfaces (PESs) and the intricate rovibrational dynamics on them, which exhibits large nuclear quantum effects. However, decoding this information for any molecular complex of interest is a demanding task, whose accomplishment involves, on the theoretical side, *ab initio* electronic structure calculation of an accurate high-dimensional (ideally, a full-dimensional) PES and rigorously computing the (ro)vibrational eigenstates of the complex on this PES. Comparison between the theoretical results thus obtained with the measured spectra permits the assignment of the latter, as well as the assessment of the quality of the PES employed and its improvement, if necessary.

This approach is feasible only if the methodology is available for accurate and efficient quantum calculation of the rovibrational states of noncovalently bound complexes. Its development must overcome several challenges, the first of which is the high dimensionality of the vibrational problem that needs to be solved. A fully coupled treatment of all vibrational, intra- and inter-molecular, degrees of freedom (DOFs) of the complex is six-dimensional (6D) for complexes of two diatomic molecules [e.g., $(HF)_2$ and $(HCl)_2$], and it is already 12D for the smallest molecular trimers, those of three diatomic molecules [e.g., $(HF)_3$ and $(HCl)_3$]. The following additional challenges arise from the characteristics of the vibrational DOFs, in particular, intermolecular: large-amplitude motions, strong anharmonicity, and coupling among themselves and with the intramolecular monomer vibrations.

For these reasons, until a couple of years ago, rigorous quantum calculations of the (ro)vibrational states of noncovalently bound molecular complexes were restricted to binary systems, and overwhelmingly under the assumption of rigid monomers, thus taking only the intermolecular DOFs of the complexes into account.[1–5] While significantly reducing the dimensionality of the problem, the rigid-monomer approach is incapable of describing important aspects of the vibrational dynamics that involve intramolecular monomer vibrations and their excitations, e.g., intramolecular vibrational frequencies and their shifts from the gas-phase monomer values due to the complexation, as well the effects of the coupling between the intra- and inter-molecular vibrational modes. The earliest instances of the full-dimensional and fully coupled treatment of the vibrations of noncovalently bound molecular dimers were those in 6D for the HF dimer[6–8] and HCl dimer.[8–10] Subsequent rigorous full-dimensional quantum calculations of the vibrational eigenstates of such systems remained limited to molecular dimers, $(HF)_2$[11,12] and $(H_2O)_2$ (12D, including states with the excited monomer bend but not the excitations of the monomer stretches).[13]

The range of noncovalently bound binary molecular complexes, for which full-dimensional quantum calculations of fully coupled excited intra- and inter-molecular vibrational states are feasible, was significantly enlarged beyond diatom–diatom systems by our introduction of the novel computational strategy in which the eigenstates of reduced-dimension intra- and inter-molecular vibrational Hamiltonians serve as compact contracted bases for the intra- and inter-molecular DOFs, respectively, of the molecular complex.[14,15]

The use of the eigenstates of intermediate reduced-dimension Hamiltonians as compact contracted bases in full-dimensional bound-state calculations has been a long tradition. The sequential diagonalization-truncation method of Bačić and Light[16–19] was very successfully applied to floppy isomerizing molecules, e.g., LiCN/LiNC and HCN/HNC, as well as weakly bound molecular complexes. On the other hand, Carrington and co-workers[20–23] have developed approaches in which the internal coordinates of (covalently bound) polyatomic molecules are divided in two groups, referred to as stretch and bend, and contracted basis functions are used for both groups, subject to two different energy cutoffs. However, this approach, which is rather close in spirit to ours, was not extended to noncovalently bound molecular complexes until later. Zou *et al.*,[24] in their quantum 6D calculations of the vibrational states of the isomerizing acetylene/vinylidene system, combined the eigenfunctions of the reduced-dimension 4D and 2D Hamiltonians into the final 6D basis, in which the full-dimensional vibrational Hamiltonian was diagonalized. A certain number of the intermediate 4D eigenstates below and above the lowest-energy (4D) vinylidene state was included in the 6D basis.

The key to the success of our strategy[14,15] was the insight[25] that in noncovalently bound molecular systems, the coupling between the high-frequency intramolecular modes and the low-frequency intermolecular vibrations is very weak. Due to this weak coupling, only a relatively small number of low-energy eigenstates of the intermolecular vibrational Hamiltonian (far below the energies of the intramolecular vibrational fundamentals) needs to be included in the final product-contracted basis in order to obtain highly accurate full-dimensional vibrational energy levels of the complex. This methodology has enabled fully coupled quantum calculations, in full dimensionality (9D), of the (ro)vibrational states of water-containing binary molecular complexes for flexible monomers, H_2O/D_2O–CO,[15] HDO-CO,[26] H_2O–HCl,[27] and several of its H/D isotopologues,[28,29] benzene-H_2O/HDO (9D, flexible water and rigid benzene),[30] $H_2O@C_{60}$ (9D, flexible water and rigid C_{60}),[31] and, most recently, the water dimer (12D), including the excited OH-stretch states.[32] For the first time, these calculations have yielded all intramolecular vibrational fundamentals and their frequency shifts, as well as the low-energy intermolecular vibrational states in each of the intramolecular vibrational manifolds and the effects of the coupling between the two sets of modes. A recent comprehensive review of these methodological developments and their applications to binary molecular complexes is available.[33]

For a cluster of molecules, the total PES is commonly represented by a many-body expansion as the sum of one-body (monomer), two-body, three-body, and possibly higher-body interactions. The procedure described above has been proven to be capable of generating a full-dimensional two-body potential for a pair of molecules. However, while the two-body terms are dominant, it is well known that the nonadditive three-body interactions make a significant contribution and have to be included for an accurate representation of the total PES of a molecular cluster. The smallest clusters, for which the three-body interactions can manifest, are molecular trimers. Therefore, in principle, noncovalently bound molecular trimers can play the same role in quantifying the three-body interactions that molecular dimers have had for a long time in determining the two-body interactions. However, just as for dimers, the realization of this potential presupposes the existence of rigorous, ideally full-dimensional quantum calculations of the vibrational eigenstates (intra- and inter-molecular) of the molecular

trimer of interest, on an *ab initio* calculated PES, and the comparison of the results with the spectroscopic data. The problem with this was that until very recently, the bound-state methodology required for accomplishing this task in the case of hydrogen-bonded molecular trimers simply was not available.

This situation changed when Felker and Bačić recently implemented the strategy outlined above, which proved successful for noncovalently bound binary molecular complexes,[14,15,33] in the methodology that has enabled the first rigorous quantum calculations of the vibrational states of a hydrogen-bonded molecular trimer, in this case of diatomic molecules, initially in 9D for rigid monomers[34] and then in full dimensionality (12D), for flexible monomers.[35] In the 12D calculations of the fully coupled excited intra- and inter-molecular vibrational states of the molecular trimer, the full vibrational trimer Hamiltonian, largely derived by Wang and Carrington,[36] is partitioned into two reduced-dimension Hamiltonians, one in 9D for the intermolecular vibrational DOFs and another in 3D for the intramolecular vibrations of the trimer and a remainder term. These two Hamiltonians are diagonalized separately and a fraction of their respective 9D and 3D eigenstates is included in the 12D product contracted basis for both the intra- and inter-molecular DOFs, in which the matrix of the full 12D vibrational Hamiltonian of the trimer is diagonalized.[35] Thanks to this methodological development, it is now possible to calculate the inter- and intra-molecular vibrational levels of hydrogen-bonded trimers of diatomic molecules in full dimensionality and with the degree of rigor that was previously feasible only for the binary molecular complexes.

In Ref. 35, this methodology was applied to the 12D calculations of the vibrational states of $(HF)_3$, which included the one- and two-quanta intramolecular HF-stretch excited vibrational states of the trimer and low-energy intermolecular vibrational states in these intramolecular vibrational manifolds. The 2 + 3-body SO-3 + HF3BG PES of HF trimer[37,38] was employed in these calculations.

Here, the same methodology[35] is used to compute, for the first time, fully coupled, full-dimensional (12D) excited intra- and inter-molecular vibrational states of $(HCl)_3$, another hydrogen-bonded molecular trimer of fundamental importance. As in $(HF)_3$, each monomer of $(HCl)_3$ is both the proton donor and proton acceptor, creating a cyclic structure with nonlinear hydrogen bonds. To date, there have been no such rigorous bound-state calculations of this molecular trimer, whose vibrational dynamics, like that of $(HF)_3$, has been the subject of numerous experimental and theoretical studies.

Bevan and co-workers[39] measured the high-resolution rovibrational spectrum of the asymmetric intramolecular HCl ν_5 vibrational band of the HCl trimer in supersonic jet expansion. They showed that the observed spectrum could be understood in terms of an oblate rovibrator model, whose structure is consistent with $(HCl)_3$ in the ground state having a dynamically averaged planar geometry. Moreover, they provided both theoretical and experimental evidence, indicating that the tunneling between the clockwise (cw) and counterclockwise (ccw) forms of the trimer is negligible. Nesbitt and co-workers[40,41] investigated various isotopologues of $(HCl)_3$ by means of high-resolution IR spectroscopy in supersonic slit expansion, obtaining detailed dynamical and structural information. This allowed them to assign the asymmetric HCl stretch vibration in the isotopologues of the trimer. In addition, the measured homogeneous line broadening was interpreted in terms of intramolecular vibrational redistribution-induced opening of the trimer ring, followed by true predissociation. A combined experimental and theoretical study of the vibrational predissociation of $(HCl)_3$ by Reisler, Bowman, and co-workers[42] determined the dissociation energies for breaking two hydrogen bonds (leading to dimer + monomer fragments) and all three hydrogen bonds (generating three monomer fragments) of the trimer, and rotational distributions of HCl fragments, as well as provided insight into the mechanism of the trimer fragmentation. In addition to these gas-phase studies, Engdahl and Nelander[43] performed Ne matrix isolation spectroscopic measurements for different H/D isotopologues of the HCl trimer and assigned two peaks at 229.9 and 239.3 cm^{-1} to the intermolecular out-of-plane symmetric bend and in-plane asymmetric bend fundamental of HCl trimer, respectively.

On the theoretical side, Latajka and Scheiner[44] studied the energetics, structure, and harmonic vibrational frequencies of the HCl trimer, as well as the dimer and tetramer (and those of other hydrogen halides) by *ab initio* electronic structure calculations. They also investigated cooperative, many-body effects in the hydrogen bonding of these systems.

Going beyond the harmonic treatment of cluster vibrations, Mancini and Bowman[45] performed *on-the-fly ab initio* calculations of the anharmonic intramolecular vibrational frequencies of $(HCl)_n$ $(n = 2–6)$ clusters. The local-monomer model (LMon) was employed in these calculations. The LMon approach is powerful and versatile, but it does not include low-frequency intermolecular modes and their coupling to the high-frequency intramolecular vibrations.

In this paper, we report rigorous 12D quantum calculations of the coupled intra- and inter-molecular vibrational states of the HCl trimer, together with the frequency shifts of the former from those of the isolated HCl monomer. These calculations are performed on the many-body PES of the trimer developed by Mancini and Bowman,[46] which includes one-, two-, and three-body interactions. The 12D PES is constructed from an already available accurate semiempirical monomer[47] and dimer[10] surfaces and a new high-level *ab initio* permutationally invariant 12D three-body potential. Using this PES, Mancini and Bowman have performed LMon calculations, augmented with harmonic Hückel-type mode coupling, of the anharmonic HCl stretch frequencies of the trimer.[46]

Having the 12D results from the present work allows us to assess the accuracy of reduced-dimensional models when applied to the vibrations of the HCl trimer. We also investigated the coupling between the inter- and intra-molecular vibrational modes of the trimer and the manifestations of the cooperative hydrogen bonding, resulting from the three-body interactions. The states localized in the secondary minima on the HCl trimer PES are analyzed as well.

The structure of this paper is as follows: computational details are described in Sec. II. In Sec. III, we present and discuss the results. Section IV contains the conclusions.

TABLE I. Energies and internal coordinates in the global minimum and secondary minima of the PES.[46] The energy is relative to the energy of the isolated flexible monomers in their equilibrium structure. $k \in 1, 2, 3$ denotes the index of the HCl monomers. For the global minimum, the coordinates are equal for all values of k. In the case of the secondary minima, the three numbers in the parentheses denote the coordinate values for $k = 1, 2$, and 3.

	Global minimum	Z secondary minimum	Y Secondary minimum
E (cm^{-1})	−2335.52	−1599	−1198
r_k (bohr)	2.4245	(2.4168, 2.4225, 2.4125)	(2.4124, 2.4177, 2.4124)
R_k (bohr)	6.9196	(6.9965, 7.4812, 6.9670)	(7.1351, 10.5922, 7.1325)
θ_k (°)	90.0000	(89.9151, 90.0169, 89.7451)	(79.6956, 179.6610, 79.3388)
ϕ_k (°)	47.6534	(45.2756, 40.4201, 224.8820)	(20.9535, 46.9121, 340.2355)

II. COMPUTATIONAL DETAILS

A. Potential energy surface

The many-body PES developed by Mancini and Bowman[46] is employed. This potential is expressed as a sum of one-, two-, and three-body terms. The one-body term is the spectroscopically accurate HCl monomer potential of Ref. 47, which was constructed from least-squares fits to microwave and infrared spectral lines of the isolated HCl monomer. The two-body term is obtained from the 6D ES1-EL dimer potential of Ref. 10. The ES1-EL potential is constructed from the ES1 dimer potential[48] (which was fitted to spectroscopic data) with the addition of an electrostatic term to improve the computed tunneling splittings of the HCl dimer for HCl-stretch excited states. The three-body term was obtained from a least-squares fit to ≈52000 three-body energies computed using the CCSD(T)-F12/aVDZ level of theory for structures sampled from dynamics simulation. The three-body PES is characterized by a ring-shaped global minimum structure and two secondary minima, denoted in Ref. 46 as Z and Y (see Table I). Note that potential is less reliable in the regions of secondary minima and transition states because the training data contain fewer structures in these regions.[49]

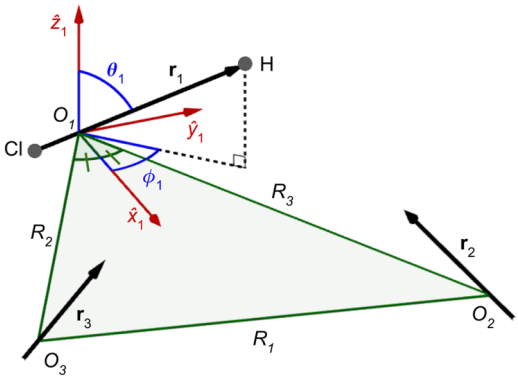

FIG. 1. Schematic depiction of the r_k, R_k, θ_k, ϕ_k (k = 1–3) coordinates used for the cyclic HCl trimer with flexible monomers. O_k (k = 1–3) is the c.m. (center of mass) of the monomer k. Shown explicitly are the three monomer-c.m. to monomer-c.m. distances R_k and the HCl internuclear vectors $\mathbf{r}_k$ (k = 1–3). The intramolecular HCl-stretch coordinate of the kth monomer is $r_k \equiv |\mathbf{r}_k|$. The ϕ_1 and θ_1 angles as well as the $\hat{x}_1$, $\hat{y}_1$, and $\hat{z}_1$ axes of the local Cartesian system centered at O_1 are also shown. For each monomer k, the $\hat{x}_k$ and $\hat{y}_k$ axes are in the $O_1O_2O_3$ plane with $\hat{x}_k$ on the bisector of the angle of the triangle at O_k, and $\hat{z}_k = \hat{x}_k \times \hat{y}_k$, i.e., perpendicular to the $O_1O_2O_3$ plane. For each monomer k, the θ_k polar and ϕ_k azimuthal angles define the orientation of $\mathbf{r}_k$ relative to the local Cartesian axis system attached to monomer k.

B. Calculation of the vibrational states of the HCl trimer

The 12D intra- and inter-molecular vibrational states of the HCl trimer are calculated rigorously as fully coupled, employing the method developed for trimers of flexible (identical) diatomic molecules and presented in Ref. 35 where it was applied to the HF trimer. This 12D approach is described in detail in Ref. 35 and in the preceding Ref. 34, where the 9D rigid-monomer version of this methodology was introduced. Therefore, here we only summarize the salient features of the approach, using the notation in Sec. II of Ref. 35, and focus on the computational details needed for understanding the rest of this paper.

The coordinate system employed, introduced by Wang and Carrington,[36] shown in Fig. 1 is the same as for the HF trimer in Ref. 35. The r_k ($k = 1, 2, 3$) intramolecular coordinates denote the HCl bond lengths, while the R_k ($k = 1, 2, 3$) frame coordinates, collectively denoted as R, refer to the monomer-c.m. to monomer-c.m. distances. The orientation of the kth monomer is described by $\omega_k \equiv (\theta_k, \phi_k)$ and k = 1–3, (collectively denoted as ω) where ϕ_k and θ_k are the in-plane and out-of-plane angles, respectively, corresponding to motion in and out of the plane determined by the c.m.-s of the monomers. The following masses were employed in the calculations: m(H) = 1.007 825 032 u and $m(^{35}\text{Cl})$ = 34.968 852 69 u.

As outlined in Sec. I, the computational methodology[35] is based on partitioning of the full (12D) vibrational Hamiltonian $\hat{H}$ of the molecular trimer into two reduced-dimensional Hamiltonians, 9D (rigid-monomer) $\hat{H}_{\text{inter}}(R, \omega; \bar{r})$ for the intermolecular DOFs, 3D $\hat{H}_{\text{intra}}(r; \bar{R}, \bar{\omega})$ for the intramolecular DOFs, and a remainder term; a bar above a symbol denotes a coordinate that is fixed. $\hat{H}_{\text{inter}}$ and $\hat{H}_{\text{intra}}$ are diagonalized separately, and a fraction of their respective 9D and 3D eigenstates is included in the 12D product-contracted basis, in which the matrix of $\hat{H}$ is diagonalized. As mentioned before, only the low-lying 9D intermolecular states are included in the 12D basis.

The 9D intermolecular eigenstates of $\hat{H}_{\text{inter}}$ are obtained with a similar partition-contraction technique.[34] $\hat{H}_{\text{inter}}$ is partitioned into

a 3D "frame" Hamiltonian $\hat{H}_F(R;\bar{\omega},\bar{r})$, a 6D "bend" Hamiltonian $\hat{H}_B(\omega;\bar{R},\bar{r})$, and a remainder term; all three terms are defined in Ref. 34. Eigenstates of $\hat{H}_F$ and $\hat{H}_B$ are used to create the 9D product contracted basis, in which $\hat{H}_{\text{inter}}$ is diagonalized.

The choices made for the values of the coordinates $(\bar{R},\bar{\omega},\bar{r})$ that are held fixed in the above-mentioned reduced-dimensional Hamiltonians are crucial because they affect the quality of the 9D and 12D product contracted bases, and therefore, the size of the final 12D basis required to give the energy levels of $\hat{H}$ with the desired level of convergence. The values of the fixed coordinates that have been tested and ultimately selected for our calculations, as well as the basis sets employed for various trimer DOFs, are specified below in Sec. III at the beginning of each subsection presenting the results for the different reduced- and full-dimension models. The tables showing the convergence of the energy levels with respect to the basis parameters are shown in the supplementary material.

The most time-consuming part of the computational procedure is obtaining the potential energy matrix elements in the 12D basis.[35] The potential energy has to be evaluated at the points of a direct product grid formed by the PODVR grid points of the frame and intramonomer coordinates and an angular grid. In order to save computational time, we eliminate those points of the angular grid where all 6D bend functions (eigenstates of $\hat{H}_B$) included in the 12D basis have negligible amplitude. This is justified by the fact that the bend functions are quite localized. The reduction inthe angular grid is quantified by a cutoff parameter, A (≥ 0): the larger A is, the more grid points are eliminated (see Sec. II D 6 of Ref. 35). A similar basic idea was implemented, in a very different context, in Ref. 50.

C. Symmetry considerations

The computer code used in the calculations utilizes the G_{12} molecular symmetry group,[51] which contains the permutations of the monomers and the spatial inversion. The point group of the equilibrium geometry of the HCl trimer is C_{3h}. Therefore, in the G_{12} symmetry model, there are two equivalent global minima on the PES, corresponding to the cw and ccw versions of the equilibrium structure. Every vibrational state is split into two states, belonging to the following irreducible representations of G_{12}: (A_1',A_2'), (A_1'',A_2''), (E',E'), and (E'',E''). However, as mentioned in Sec. I, previous spectroscopic studies of the HCl trimer[39] have found no observable tunneling splittings due to the interconversion between the cw and ccw versions of the trimer. Our present calculations also show negligible tunneling splittings of less than 0.01 cm^{-1}. Consequently, the splittings are not reported, and only a single energy value is given for each doublet. Since the tunneling cw–ccw interconversion is not feasible, the effective molecular symmetry group of the HCl trimer is G_6 (isomorphic with C_{3h}), and not G_{12}.

III. RESULTS AND DISCUSSION

A. Intermediate reduced-dimension calculations

The main goal of the calculations of the eigenstates of the reduced-dimension Hamiltonians in 3D (inter- and intramolecular), 6D, and 9D, presented in this section, is to generate compact contracted bases, in which the higher-dimensional Hamiltonians are diagonalized. However, as shown below, these results are also helpful for elucidating the coupling among different inter- and intra-molecular vibrational modes of the trimer.

1. 3D intermolecular eigenstates of $\hat{H}_F$

The 3D frame potential V_F that appears in $\hat{H}_F$ is defined in two ways, described in Secs. II B and II C of Ref. 34: (a) $V_F = V_F^{(\text{eq})}$ when the angles are fixed at their equilibrium values, $\bar{\theta} = 90^\circ$ and $\bar{\phi} = 47.6534^\circ$ and (b) $V_F = V_F^{(\text{avg})}$, which is a Gaussian-weighted-average of the potential over the angle variables [see Eq. (18) of Ref. 34]. The parameters of the Gaussian are chosen to resemble the ground-state wave function from the 6D bend calculations. Its center is $\theta_0 = 90^\circ$ and $\phi_0 = 48.5^\circ$, while the standard deviations are $\sigma_\theta = 13.7^\circ$ and $\sigma_\phi = 11.8^\circ$. Eleven points are used for the averaging, evenly distributed on the $[\theta_0 - 2.5\sigma_\theta, \theta_0 + 2.5\sigma_\theta]$ and $[\phi_0 - 2.5\sigma_\phi, \phi_0 + 2.5\sigma_\phi]$ ranges for each θ_k and ϕ_k angle, respectively.

In $\hat{H}_F$, the HCl monomer bond lengths r_k (k = 1–3) are fixed. The following three fixed values for every r_k were tested: one of them, $\bar{r}_e$ = 2.4245 bohrs, is the equilibrium value. The other two values are from the reduced-dimension quantum 3D calculations of the intramolecular vibrational eigenstates of $\hat{H}_{\text{intra}}$, $\bar{r}_0$ = 2.4569 bohrs—the expectation value of the HCl bond length in the ground vibrational state, obtained from diagonalization of $\hat{H}_{\text{intra}}$,where the intermolecular coordinates were fixed at their equilibrium values (note that this is slightly different from the expectation value obtained from the 12D computation, which is 2.452 bohrs) and $\bar{r}^\star$ = 2.4681 bohrs—the average of the expectation values of the HCl bond length in the ground and the first excited states.

Once V_F and $\bar{r}_e$ have been specified, $\hat{H}_F$ is diagonalized in the basis consisting of the products of three 1D potential-optimized discrete variable representation (PODVR)[52,53] functions covering the R_1, R_2, and R_3 intermonomer distances, respectively. The results presented here are obtained with the 3D basis of N_R = 12 PODVR functions for each R_k (k = 1, 2, 3) frame coordinate following extensive convergence tests (see Table I of the supplementary material).

Table II presents the ten lowest eigenvalues of the 3D $\hat{H}_F$, obtained with three different fixed HCl bond length values ($\bar{r}$) and the two effective potentials, $V_F^{(\text{avg})}$ and $V_F^{(\text{eq})}$. HX (X = Cl, F, ...) trimers have two frame intermolecular vibrational modes, the symmetric stretch (ν_{ss} and A_1' symmetry) and the doubly degenerate asymmetric stretch (ν_{as} and E' symmetry). The symmetric stretch has higher energy than the asymmetric stretch; the same was found[35] for $(HF)_3$. It is evident from Table II that the frame energies are sensitive to the choice of both V_F and $\bar{r}$. They increase by a few cm^{-1} as $\bar{r}$ changes from $\bar{r}_e$ to $\bar{r}_0$ and then to $\bar{r}^\star$, for both choices of V_F. Similarly, using $V_F^{(\text{avg})}$ instead of $V_F^{(\text{eq})}$ substantially lowers all frame eigenvalues, regardless of which $\bar{r}$ value is used, $\bar{r}_e$, $\bar{r}_0$, or $\bar{r}^\star$. The reason is that $V_F^{(\text{avg})}$ samples configurations with (partially) broken H-bonds, making $V_F^{(\text{avg})}$ less steep than $V_F^{(\text{eq})}$. Note that $V_F^{(\text{avg})}$ turns out to be superior to $V_F^{(\text{eq})}$ in the sense that it is more similar to the 9D eigenstates (*vide infra*) thus, yielding better 9D product basis. In addition, Table II presents the expectation values ($\langle R_k\rangle$) and the root mean square (rms) deviations (ΔR_k) of the frame coordinates for the first ten frame eigenstates obtained with $\bar{r} = \bar{r}_0$ and $V_F^{(\text{avg})}$. (See the supplementary material, Tables II and III for additional information regarding $\langle R_k\rangle$ and ΔR_k values for the excited states.)

TABLE II. Lowest eigenenergies of the 3D $\hat{H}_F$, in cm^{-1}, obtained with different $\bar{r}$ values and $V_F = V_F^{(eq)}$ or $V_F = V_F^{(avg)}$. The $\langle R\rangle(\Delta R)$ values, given in bohrs, correspond to the states calculated with $V_F = V_F^{(avg)}$ and $\bar{r}_0$. For additional information, see the text.

V_F	$V_F^{(avg)}$			$V_F^{(eq)}$				
$\bar{r}$	$\bar{r}_e$	$\bar{r}_0$	$\bar{r}^\star$	$\bar{r}_e$	$\bar{r}_0$	$\bar{r}^\star$	$\langle R\rangle(\Delta R)$	Assign.
1	0.00	0.00	0.00	0.00	0.00	0.00	7.049 (0.196)	gs (A_1')
2, 3	74.87	76.83	77.54	87.48	90.36	90.57	7.092 (0.248)	$\nu_{as}(E')$
4	93.44	95.18	95.81	107.89	110.60	110.92	7.108 (0.279)	$\nu_{ss}(A_1')$
5	146.91	150.72	152.12	171.67	177.29	177.71	7.135 (0.303)	$2\nu_{as}(A_1')$
6, 7	147.31	151.17	152.59	172.16	177.86	178.30	7.136 (0.302)	$2\nu_{as}(E')$
8, 9	163.06	166.77	168.12	189.52	195.09	195.64	7.152 (0.328)	$\nu_{ss} + \nu_{as}(E')$
10	183.07	186.58	187.84	211.58	216.99	217.64	7.169 (0.346)	$2\nu_{ss}(A_1')$

TABLE III. Lowest eigenenergies (in cm^{-1}) of $\hat{H}_B$, obtained with different $\bar{r}$ and $\bar{R}$ values (in bohrs).

$(\bar{r}, \bar{R})$ =	$(\bar{r}_e, 7.0)$	$(\bar{r}_e, 7.1)$	$(\bar{r}_e, 7.2)$	$(\bar{r}_0, 7.0)$	$(\bar{r}_0, 7.1)$	$(\bar{r}_0, 7.2)$	$(\bar{r}^\star, 7.1)$	Assignment
				A_1', A_2'				
1	0.00	0.00	0.00	0.00	0.00	0.00	0.00	gs
2	314.36	303.38	291.79	330.20	318.19	305.76	323.28	$2\nu_{oab}$
3	373.31	359.36	345.44	380.93	366.74	352.62	369.21	ν_{isb}
4	440.57	424.39	407.70	455.63	437.52	419.37	441.75	$2\nu_{iab}$
5	453.91	436.43	419.67	469.15	451.95	435.27	457.57	$2\nu_{osb}$
				E_a', E_b'				
1, 2	227.09	217.39	207.95	232.76	222.67	212.92	224.49	ν_{iab}
3, 4	325.20	314.08	302.37	341.22	329.10	316.57	334.25	$2\nu_{oab}$
5, 6	377.69	364.64	351.16	395.02	381.01	366.71	386.62	$\nu_{osb} + \nu_{oab}$
7, 8	444.29	425.13	406.42	455.93	435.97	416.63	439.69	$2\nu_{iab}$
13, 14	568.56	545.06	521.52	585.11	560.59	536.31	565.63	$\nu_{isb} + \nu_{iab}$
				A_1'', A_2''				
1	223.59	216.31	208.88	233.76	226.04	218.24	229.34	ν_{osb}
2	376.34	361.65	346.73	391.03	375.32	359.59	379.99	$\nu_{iab} + \nu_{oab}$
3	395.00	379.55	364.03	408.85	392.51	376.28	396.92	$\nu_{iab} + \nu_{oab}$
4	470.10	453.08	435.32	493.08	474.72	455.83	482.20	$3\nu_{oab}$
5	481.19	464.93	447.74	504.11	486.37	467.95	493.77	$3\nu_{oab}$
7	571.43	549.38	526.80	591.04	568.26	545.05	574.65	$\nu_{isb} + \nu_{osb}$
				E_a'', E_b''				
1, 2	166.88	161.24	155.30	175.13	168.97	162.60	171.61	ν_{oab}
3, 4	383.05	367.94	352.71	397.18	381.16	365.18	385.67	$\nu_{iab} + \nu_{oab}$
5, 6	437.50	420.78	404.09	453.28	435.70	418.30	440.81	$\nu_{iab} + \nu_{osb}$
7, 8	455.00	438.67	421.49	477.62	459.83	441.43	467.16	$3\nu_{oab}$
9, 10	520.15	501.32	481.93	540.95	520.70	500.23	526.66	$\nu_{isb} + \nu_{oab}$

The ground-state expectation value of R_k is about 0.13 bohrs larger than the equilibrium value due to the wave function averaging, as expected. For the excited states, the values of both $\langle R_k\rangle$ and ΔR_k increase further with the number of quanta.

2. 6D intermolecular eigenstates of $\hat{H}_B$

For 6D $\hat{H}_B$, it is necessary to specify the fixed intermonomer distance $\bar{R}$ and the (also fixed) HCl bond length $\bar{r}$. In the calculations of the eigenstates of $\hat{H}_B$, based on consideration of the expecta-

TABLE IV. Properties of the lowest-energy 6D eigenstates of $\hat{H}_B$ for $\bar{R}$ = 7.1 bohrs and $\bar{r} = \bar{r}_0$. The ΔE values are in cm^{-1}, while $\langle\phi_k\rangle$, $\Delta\phi_k$, and $\Delta\theta_k$ are in degrees. For all states, $\langle\theta_k\rangle = 90°$ for symmetry reasons.

	ΔE	$\langle\phi_1\rangle(\Delta\phi_1)$	$\langle\phi_3\rangle(\Delta\phi_3)$	$\langle\phi_3\rangle(\Delta\phi_3)$	$(\Delta\theta_1, \Delta\theta_2, \Delta\theta_3,)$	Assignment
			A_1', A_2'			
1	0.00	48.6 (11.7)	48.6 (11.7)	48.6 (11.7)	(13.5, 13.5, 13.5)	gs
2	318.19	47.4 (13.5)	47.4 (13.5)	47.4 (13.5)	(22.3, 22.3, 22.3)	$2\nu_{\text{oab}}$
3	366.74	50.1 (15.8)	50.1 (15.8)	50.1 (15.8)	(14.6, 14.6, 14.6)	ν_{isb}
			E_a', E_b'			
1	222.67	49.3 (18.3)	49.2 (14.6)	49.2 (14.6)	(13.8, 14.1, 14.1)	ν_{iab}
2	222.67	49.2 (13.2)	49.3 (17.2)	49.3 (17.2)	(14.3, 13.9, 13.9)	ν_{iab}
3	329.10	47.3 (12.9)	47.9 (13.2)	47.9 (13.2)	(20.7, 23.0, 23.0)	$2\nu_{\text{oab}}$
4	329.10	48.1 (13.3)	47.5 (13.0)	47.5 (13.0)	(23.7, 21.5, 21.5)	$2\nu_{\text{oab}}$
			A_1'', A_2''			
1	226.04	49.2 (12.4)	49.2 (12.4)	49.2 (12.4)	(17.4, 17.4, 17.4)	ν_{osb}
4	474.72	47.3 (14.3)	47.3 (14.3)	47.3 (14.3)	(26.3, 26.3, 26.3)	$3\nu_{\text{oab}}$
5	486.37	47.1 (14.0)	47.1 (14.0)	47.1 (14.0)	(25.7, 25.7, 25.7)	$3\nu_{\text{oab}}$
			E_a'', E_b''			
1	168.97	48.1 (12.6)	48.1 (12.2)	48.1 (12.2)	(21.7, 16.1, 16.1)	ν_{oab}
2	168.97	48.2 (12.1)	48.1 (12.5)	48.1 (12.5)	(13.7, 20.0, 20.0)	ν_{oab}
7	459.83	46.8 (15.8)	46.6 (14.4)	46.6 (14.4)	(32.3, 22.5, 22.5)	$3\nu_{\text{oab}}$
8	459.83	46.6 (13.9)	46.8 (15.3)	46.8 (15.3)	(18.2, 29.4, 29.4)	$3\nu_{\text{oab}}$

tion values $\langle R_k\rangle$ for the lowest-energy 3D frame eigenstates in the supplementary material, Tables II and III, we decided to test $\bar{R}$ = 7.0, 7.1 and 7.2 bohrs, together with the three $\bar{r}$ values, $\bar{r}_e$, $\bar{r}_0$, and $\bar{r}^\star$, defined in Sec. III A 1. The 6D bend eigenstates of $\hat{H}_B$ are computed on the basis consisting of the products of spherical harmonics $Y_m^l(\theta,\phi)$, and all spherical harmonics with $l \le l_{\max} = 13$ are included in the final calculations.

Table III presents the first few eigenvalues of $\hat{H}_B$ for the $\bar{R}$ and $\bar{r}$ values employed (convergence test is presented in Table IV of the supplementary material). The eigenvalues of $\hat{H}_B$ appear as closely spaced tunneling doublets because the calculations sample two equivalent minima on the PES, corresponding to the clockwise and counter-clockwise versions of the equilibrium structure. (There is no tunneling splitting for the eigenvalues of $\hat{H}_F$ because in that case, the angular coordinates are fixed so that only one minimum is sampled.) The computed tunneling splittings are less than 0.01 cm^{-1} for the bending states investigated here, and therefore, only one energy value is provided for each of the $A_1^s - A_2^s$ and $E^s - E^s$ ($^s = {}'$ or $''$) state pairs. (Note that for the E^s symmetry, we obtain four numerically nearly degenerate eigenvalues since E^s is doubly degenerate and all eigenvalues are duplicated due to the permutation-inversion symmetry.)

The bending modes of the HX trimers are as follows: in-plane symmetric bend (ν_{isb}, A_1', and A_2'), in-plane asymmetric bend (ν_{iab} and two doubly degenerate E' states), out-of-plane symmetric bend (ν_{osb}, A_1'', and A_2''), and the out-of-plane asymmetric bend (ν_{oab} and two doubly degenerate E'' states). The $\bar{R}$ and $\bar{r}$ dependence of the 6D bending energies presented in Table III reflects the coupling of the bending vibrations with the inter- and intra-molecular stretching vibrations, respectively. Two trends regarding the bending energies are evident: (a) they decrease with increasing $\bar{R}$ due to the decreasing angular anisotropy of the PES as the intermonomer distances increase. (b) They increase with increasing $\bar{r}$. This is caused by the monomer–monomer "crowding" effect, which increases with increasing H-X bond length.

Table IV presents the expectation values ($\langle\phi_k\rangle$) and the rms deviations ($\Delta\phi_k, \Delta\theta_k$) of the angle coordinates for the selected 6D bend eigenstates, obtained with $\bar{r} = \bar{r}_0$ and $\bar{R}$ = 7.1 bohrs (Table V of the supplementary material shows these quantities for all the states in Table III.) We used the ground-state expectation values and the root-mean-square deviations to parameterize $V_F^{(\text{avg})}$ in the 3D frame calculations. The in-plane bending modes are characterized by large $\Delta\phi_k$ values, while $\Delta\theta_k$ is large for the out-of-plane vibrations. For most excited states investigated here, $\langle\phi_k\rangle$ is slightly larger than in the ground state. However, $\langle\phi_k\rangle$ is slightly smaller for ν_{oab} than for the ground state and further decreases for the higher excitations of this mode, reaching 46.8° for $3\nu_{\text{oab}}$.

3. 9D intermolecular eigenstates of $\hat{H}_{inter}$

The 9D calculations described in this section are analogous to our earlier 9D rigid-monomer calculations of the intermolecular vibrational states of the HF trimer.[34] The supplementary material, Tables VII, VIII, and IX, present how the 9D intermolecular vibrational eigenenergies of $\hat{H}_{\text{inter}}$ vary with respect to the following

TABLE V. Energies (in cm^{-1}) of selected intermolecular vibrational eigenstates of the HCl trimer from 9D rigid-monomer calculations of the HCl trimer, computed for three different $\bar{r}$ values. The energies of the corresponding intermolecular vibrational states from the full-dimensional (12D) calculations, for the ground intramolecular vibrational state, are shown as well. *: low basis state norm (see the text).

	A_1', A_2'					E'			
	9D, $\bar{r}_e$	9D, $\bar{r}_0$	9D, $\bar{r}^*$	12D		9D, $\bar{r}_e$	9D, $\bar{r}_0$	9D, $\bar{r}^*$	12D
gs	0.00	0.00	0.00	0.00	ν_{as}	72.72	75.53	76.57	75.94
ν_{ss}	90.91	93.56	94.52	93.29	$2\nu_{as}$	141.95	147.48	149.51	148.28
$2\nu_{as}$	141.17	146.62	148.63	147.15	$\nu_{ss} + \nu_{as}$	157.78	163.23	165.22	163.66
$2\nu_{ss}$	177.67	183.01	184.93	182.60	ν_{iab}	219.05	226.76	229.51	228.55
$\nu_{as} + \nu_{iab}$	284.98	295.54	299.36	296.80	$\nu_{as} + \nu_{iab}$	287.20	297.67	301.46	299.29
$\nu_{as} + \nu_{iab}$	288.25	298.66	302.41	300.43	$\nu_{ss} + \nu_{iab}$	304.49	314.94	318.65	316.40
$2\nu_{oab}$	299.12	316.85	323.11	315.48	$2\nu_{oab}$	310.14	328.28	334.46	328.34
ν_{isb}	361.83	373.04	377.04	374.3[a]	$\nu_{osb} + \nu_{oab}$*	367.60	387.16	394.17	⋯
$2\nu_{osb}$*	439.12	460.69	468.20	⋯	$\nu_{as} + \nu_{isb}$	431.61	445.73	451.00	446.99
	A_1'', A_2''					E''			
	9D, $\bar{r}_e$	9D, $\bar{r}_0$	9D, $\bar{r}^*$	12D		9D, $\bar{r}_e$	9D, $\bar{r}_0$	9D, $\bar{r}^*$	12D
ν_{osb}	213.72	225.55	229.67	225.02	ν_{oab}	160.15	169.44	172.69	169.22
$\nu_{as} + \nu_{oab}$	228.01	239.74	243.87	239.60	$\nu_{as} + \nu_{oab}$	228.43	240.38	244.60	240.48
$\nu_{as} + \nu_{oab}$	232.64	244.59	248.82	244.53	$\nu_{ss} + \nu_{oab}$	247.50	259.36	263.52	259.11
$\nu_{ss} + \nu_{osb}$	301.40	315.71	320.73	315.28	$\nu_{iab} + \nu_{oab}$	367.33	384.27	390.20	385.16
$\nu_{iab} + \nu_{oab}$	359.13	376.46	382.56	377.31	$\nu_{iab} + \nu_{osb}$*	416.42	435.76	442.58	⋯
$\nu_{iab} + \nu_{oab}$	377.38	394.18	400.09	395.31	$3\nu_{oab}$*	428.00	455.50	464.71	⋯
$3\nu_{oab}$	441.41	468.14	477.67	466.02	$\nu_{isb} + \nu_{oab}$*	497.38	524.10	⋯	⋯
$3\nu_{oab}$	459.09	484.68	493.63	483.62					
$\nu_{isb} + \nu_{osb}$	548.19	572.67	581.15	572.27					

[a] Average energy of the two candidate states, 373.96 cm^{-1} and 374.72 cm^{-1}.

parameters: the number of eigenstates of $\hat{H}_B$ *per subirrep* included in the 9D basis (N_B), the number of eigenstates of $\hat{H}_F$ included in the 9D basis (N_F), N_R, and $\bar{R}$. They also show the effect of using $V_F^{(avg)}$ or $V_F^{(eq)}$ when computing the eigenstates of $\hat{H}_F$. Based on this information, the calculations of the 9D eigenstates of $\hat{H}_{inter}$ are performed using $\bar{R}$ = 7.1 bohrs, $V_F = V_F^{(avg)}$, N_B = 30, N_F = 150, and N_R = 12. We choose $V_F = V_F^{(avg)}$ because the eigenstates of the 3D $\hat{H}_F$ computed with $V_F^{(avg)}$ are closer in energy to the corresponding frame eigenstates of 9D $\hat{H}_{inter}$ than those obtained using $V_F^{(eq)}$. Furthermore, comparison of the energies of the bending vibrations from the 9D calculations (eigenstates of $\hat{H}_{inter}$) to those from the 6D bending-level calculations (eigenstates of $\hat{H}_B$) reveals that the agreement is the best for 6D eigenenergies obtained using $\bar{R}$ = 7.1 bohrs, suggesting that this is the optimal $\bar{R}$ value.

Table V presents the intermolecular vibrational energy levels computed in the 9D model for three different $\bar{r}$ values, $\bar{r}_e$, $\bar{r}_0$, or $\bar{r}^*$, specified in Sec. III A 1. We show only those states whose dominant basis-state norm (BSN) is greater than 0.4 and that have, at most, two vibrational quanta (and $3\nu_{oab}$). The states that have a lower BSN (around 0.3) but could still be identified unambiguously are denoted with an asterisk. Table V also presents the selected 12D eigenstates of $\hat{H}$ for the monomers in their ground intramolecular vibrational states, which are discussed in more detail in Sec. III B. It is evident from Table V that the 9D excitation energies are sensitive to the value of the monomer bond length $\bar{r}$ used in the calculations, i.e., they increase significantly as the HCl bond length increases. This demonstrates that, just as in the case of the HF trimer,[34,35] the coupling of inter- and intra-molecular vibrational modes is not negligible and can be fully accounted for only by rigorous 12D calculations. In general, the energies of the bending vibrations increase more with increasing HCl bond length than those of the frame vibrations, suggesting that the inter–intra coupling is larger for the bending modes than for the frame modes.

Table VI presents the expectation values and the root-mean-square (rms) deviations of the coordinates calculated for selected eigenstates of the 9D intermolecular Hamiltonian, for $\bar{r} = \bar{r}_0$. The quantities $\langle q \rangle$ and Δq ($q = R, r, \phi$ or θ) are calculated by averaging the $\langle q_k \rangle$ and Δq_k values for $k = 1, 2, 3$ and for all nearly degenerate states corresponding to a given vibrational state, i.e., two wave functions for vibrations with A' (A'') symmetry and four wave functions for vibrations with E' (E'') symmetry. In the case of the frame vibrations, $\langle R \rangle$ and ΔR are similar to the corresponding values calculated in the 3D frame model (see Table II), while the expectation values and rms deviations of the angle coordinates are very similar to the ground state values, probably because the frame

TABLE VI. Properties of selected inter- and intra-molecular vibrational eigenstates of the full 12D Hamiltonian and the 9D intermolecular Hamiltonian with $\bar{r} = \bar{r}_0$. $\langle q \rangle$ and Δq ($q = R, r, \phi$ or θ) are calculated by averaging the $\langle q_k \rangle$ and Δq_k values for $k = 1, 2, 3$ and for all nearly degenerate states corresponding to a given vibrational state, i.e., two wave functions for vibrations with A' (A'') symmetry and four wave functions for vibrations with E' (E'') symmetry.

	12D				9D		
	$\langle r \rangle (\Delta r)$	$\langle R \rangle (\Delta R)$	$\langle \phi \rangle (\Delta \phi)$	$(\Delta \theta)$	$\langle R \rangle (\Delta R)$	$\langle \phi \rangle (\Delta \phi)$	$(\Delta \theta)$
gs	2.452 (0.147)	7.040 (0.197)	48.4 (11.7)	(13.5)	7.043 (0.197)	48.5 (11.7)	(13.4)
ν_{as}	2.451 (0.147)	7.088 (0.251)	48.6 (11.9)	(13.7)	7.090 (0.251)	48.6 (11.8)	(13.5)
ν_{ss}	2.451 (0.147)	7.104 (0.283)	48.6 (11.9)	(13.7)	7.106 (0.283)	48.6 (11.8)	(13.6)
ν_{oab}	2.450 (0.146)	7.065 (0.203)	48.1 (12.4)	(18.1)	7.066 (0.203)	48.1 (12.4)	(17.8)
ν_{osb}	2.450 (0.146)	7.088 (0.224)	49.0 (12.6)	(17.9)	7.089 (0.224)	48.9 (12.5)	(17.7)
ν_{iab}	2.451 (0.146)	7.090 (0.226)	49.2 (15.5)	(14.1)	7.088 (0.219)	49.2 (15.6)	(14.0)
ν_{isb} [a]	2.450 (0.146)	7.232 (0.448)	49.6 (14.9)	(14.9)	7.166 (0.348)	49.8 (15.3)	(14.6)
ν_{sym}^{HCl}	2.474 (0.194)	7.011 (0.202)	48.1 (11.4)	(13.1)	⋯	⋯	⋯
ν_{asym}^{HCl}	2.474 (0.190)	7.022 (0.195)	48.2 (11.5)	(13.2)	⋯	⋯	⋯

[a]The 12D values are averaged for the two candidate states.

vibrations have low energy. In the case of the bend states, $\langle \phi \rangle$, $\Delta \phi$, and $\Delta \theta$ are similar to the corresponding values in the 6D bend model (see Table IV).

An issue that one may wish to consider having the 9D results is the extent of the coupling between the intermolecular stretching (frame) vibrations and the bending vibrational modes of the HCl trimer. This coupling is rigorously included in the 9D treatment but not in either the 6D bend or the 3D frame calculations. Hence, the comparison of the 9D results with those from the 6D and 3D calculations, respectively, should, in principle, be able to shed light on the intermolecular stretch-bend coupling in this complex. For this purpose, Table VII presents the energies of the intermolecular stretching and bending vibrations from the 9D, 6D, and 3D calculations. In the case of the intermolecular frame modes, the 3D energies are slightly higher than their 9D counterparts. For the bending fundamentals, the 6D calculations mostly give slightly lower energies than the 9D treatment. Overall, the 9D results are close to the results of both the 3D frame and 6D bend calculations, with their differences not exceeding 1.8%. Based on this, one is tempted to conclude that the intermolecular stretch-bend coupling in the HCl trimer is very weak. However, the issue is not so straightforward because the 3D frame and the 6D bend contracted bases that comprise the 9D product basis are not generated in a completely independent manner. As explained in Sec. III A 1, the 3D frame potential $V_F = V_F^{(avg)}$ that appears in $\hat{H}_F$ is based on the information from the 6D bend ($\hat{H}_B$) calculations. In turn, as described in Sec. III A 2, the fixed intermonomer distance $\bar{R}$ that enters the 6D $\hat{H}_B$ is based on the expectation values $\langle R_k \rangle$ from the 3D frame ($\hat{H}_F$) calculations. Thus, the apparent weak intermolecular stretch-bend coupling that emerges from the 9D calculations is somewhat deceptive. It is at least, in part, due to the manner in which each of two reduced-dimension Hamiltonians, $\hat{H}_F$ and $\hat{H}_B$, is defined, by making use of the information based on the eigenstates of the other Hamiltonian. The frame-bend coupling would very likely appear to be larger if the parameters defining $\hat{H}_F$ and $\hat{H}_B$ were fixed independently, without sharing key information.

TABLE VII. Energies of the intermolecular vibrational fundamentals (in cm^{-1}) computed from the 9D intermolecular, 3D frame, and 6D bend calculations, all for $\bar{r} = \bar{r}_0$.

	9D	3D frame ($V_F^{(avg)}$)	6D bend ($\bar{R}$ = 7.1 bohrs)
ν_{as}	75.53	76.83	
ν_{ss}	93.56	95.18	
ν_{oab}	169.44		168.97
ν_{osb}	225.55		226.04
ν_{iab}	226.76		222.67
ν_{isb}	373.04		366.74

4. 3D intramolecular eigenstates of $\hat{H}_{intra}$

Table VIII presents several lowest intramolecular eigenstates of the 3D $\hat{H}_{intra}$, for $V_{intra} = V_{intra}^{(eq)}$ and $V_{intra} = V_{intra}^{(avg)}$ cases, obtained with $N_r = 8$ PODVR basis functions for each monomer. In the case of $V_{intra}^{(eq)}$, the intermolecular coordinates are fixed to their equilibrium values (see Table I), while for $V_{intra}^{(avg)}$, $\bar{R}_k = 7.1$ bohrs, $\bar{\phi}_k = 50°$, and $\bar{\theta}_k = 90°$ are employed, based on the expectation values obtained from the 9D intermolecular eigenstates of $\hat{H}_{inter}$. The convergence of the intramolecular eigenenergies with respect to N_r is shown in the supplementary material, Table X. Table VIII presents the corresponding intramolecular energy levels from the 12D calculation for comparison and discussion in Sec. III B.

In general, the energies of the 3D intramolecular eigenstates presented in Table VIII obtained with $V_{intra}^{(avg)}$ are higher than those computed for $V_{intra}^{(eq)}$. This implies that the hydrogen bonding in the trimer is weaker when $V_{intra}^{(avg)}$ is used, resulting in smaller redshifts of the HCl-stretch vibrations.

TABLE VIII. Energies (in cm^{-1}) of the $v = 1, 2$ HCl-stretching states of the HCl trimer computed in 12D (for intermolecular modes in the ground state) and from the 3D intramolecular Hamiltonian $\hat{H}_{intra}$. The $\langle r \rangle$ and Δr values (in bohrs) are also shown for the "3D, $V_{intra}^{(eq)}$" eigenstates (the values for the "3D, $V_{intra}^{(avg)}$" case are very similar).

	Irrep	12D	3D, $V_{intra}^{(avg)}$	3D, $V_{intra}^{(eq)}$	$\langle r \rangle(\Delta r)$
gs	A_1'	0.0	0.0	0.0	2.457 (0.147)
ν_{sym}^{HCl}	A_1'	2819.17	2811.68	2787.44	2.479 (0.194)
ν_{asym}^{HCl}	E'	2835.88	2828.85	2812.96	2.479 (0.191)
$2\nu_{sym}^{HCl}$	A_1'	5544.02	5533.81	5491.05	2.502 (0.236)
$\nu_{sym}^{HCl} + \nu_{asym}^{HCl}$	E'	5546.10	5535.75	5495.19	2.502 (0.229)
$2\nu_{asym}^{HCl}$	A_1'	5650.73	5636.46	5596.77	2.501 (0.229)
$2\nu_{asym}^{HCl}$	E'	5663.41	5650.55	5615.95	2.501 (0.227)

B. 12D intra- and inter-molecular vibrational eigenstates of $\hat{H}$

The 12D eigenstates of the full vibrational Hamiltonian presented in this section are obtained with the following parameters: the 12D product basis is built from $N_{inter} = 150$ 9D intermolecular eigenstates *for each subirrep* and $N_{intra} = 38$ 3D intramolecular eigenstates (for all states up to four vibrational quanta in the intramolecular modes). The 3D intramolecular eigenstates are calculated with $N_r = 8$ and $V_{intra} = V_{intra}^{(eq)}$, while the 9D intermolecular eigenstates are calculated with $\tilde{r} = \tilde{r}_0$, $\tilde{R} = 7.1$ bohrs, $V_F = V_F^{(avg)}$, $N_B = 30$, $N_F = 150$, and $N_R = 12$. Two values of the angular grid cutoff parameter A were tested, $A = 1.0$ and $A = 30.0$, which reduced the grid to about 15% and 7% of its original size, respectively. (Note that $A = 0.1$ was used for the HF trimer in Ref. 35, where the size of the grid was reduced to 7% of the original.) $A = 30.0$ turned out to be too large because the energy levels computed with $\tilde{r} = \tilde{r}_e$ and $\tilde{r}_0$ were slightly different; therefore, the cutoff parameter was reduced. The discrepancy between the $\tilde{r} = \tilde{r}_e$ and $\tilde{r}_0$ results becomes minuscule for $A = 1.0$, and the energies are similar to the values computed with $A = 30.0$ and $\tilde{r} = \tilde{r}_e$, showing that $A = 1.0$ is appropriate. Therefore, $A = 1.0$ is employed for all calculations reported here.

1. Intermolecular vibrations

Table V presents the energies of the selected low-lying intermolecular vibrational states of the HCl trimer from the full-dimensional (12D) calculations for the monomers in their ground intramolecular vibrational states. Here, those 12D eigenstates are listed for which the 9D eigenstates included in the basis have BSN ≥0.4. Note that there are two candidates for ν_{isb}, so we present the average of the two values. It is evident that for nearly all the states shown, the best agreement between the results of the 12D and 9D calculations is achieved when $\tilde{r} = \tilde{r}_0$ is used in the latter. In this case, the agreement for most 12D and 9D states is within a few tenths of cm^{-1} and better than 2 cm^{-1} for all states presented in Table V. Thus, when the monomers are in their ground intramolecular vibrational states, the intermolecular vibrational eigenenergies from the rigid-monomer 9D calculations (with carefully chosen $\tilde{r}$) can agree very well with those from the full-dimensional 12D calculations of the HCl trimer. However, it should be noted that the vibrationally averaged HCl bond length employed in the present 9D calculations is not that for the isolated HCl monomer but is the ground-state value from the 3D intramolecular vibrational calculation (diagonalization of 3D $\hat{H}_{intra}$). Therefore, it partially includes the effect of the hydrogen bonding in the trimer on the HCl bond length. It should also be pointed out that in the case of the HF trimer,[35] the intermolecular vibrational energy levels from the 9D and 12D calculations do not agree so well, typically differing by 1–4 cm^{-1}, but the differences can go up to 7 cm^{-1}. This suggests that the coupling between the intra- and inter-molecular vibrations is stronger for $(HF)_3$ than $(HCl)_3$, rendering the rigid-monomer treatment less accurate.

Table VI presents the expectation values and rms deviations of the coordinates for the selected inter- and intra-molecular vibrational states of the HCl trimer from 12D calculations (and also in 9D). For the ground and excited intramolecular vibrational states listed, the 12D values of $\langle r \rangle$ and Δr are very slightly smaller than those obtained from the 3D intramolecular vibrational calculations (see Table VIII). The expectation values and rms deviations of the intermolecular coordinates are generally similar in the 12D and 9D models. The exception is the ν_{isb} state, for which the 12D ΔR is considerably larger than that from the 9D calculations. [Note that the 12D value may not be reliable because there are two candidates for this state, for which the average is reported. For the candidate state at 373.96 cm^{-1}, $\langle R \rangle(\Delta R) = 7.299(0.525)$ bohrs, while for the state at 374.72 cm^{-1}, $\langle R \rangle(\Delta R) = 7.164(0.370)$ bohrs.]

Now, let us compare the 12D intermolecular vibrational energies of HCl trimer to those of the HF trimer,[35] when the monomers (HCl and HF) are in their ground intramolecular vibrational states. The energies of the intermolecular stretching vibrations are significantly lower for the HCl trimer than for the HF trimer;[35] for ν_{ss}, 93.3 vs 186.90 cm^{-1} and for ν_{as}, 75.9 vs 170.9 cm^{-1}. This is not surprising and can be mainly attributed to the fact that HCl is heavier than HF, although the differences in the potentials of the two systems must also play a role. The energies of the intermolecular bending vibrations of the HCl trimer are also lower than those of their counterparts in the HF trimer.[35] In this case, the difference between the masses of HCl and HF does not have a large effect since the bending vibrations primarily involve the large-amplitude motions of the light H atoms, while the heavy Cl and F atoms move much less. This means that the angular anisotropy of the potential for the motions of the H atoms must be considerably smaller for the HCl trimer than for the HF trimer. This is not surprising, given that the vibrationally averaged ground-state intermonomer distance in the HCl trimer, 7.04 bohrs, is greater than the corresponding intermonomer distance in the HF trimer,[35] 4.9 bohrs. Similar to the HF trimer, the lowest-energy bending fundamental of the HCl trimer is ν_{oab} and the highest-energy one is ν_{isb}. However, while the ν_{iab} and ν_{osb} fundamentals have very similar energies for the HCl trimer, this is not the case with the HF trimer.[35]

Spectroscopic data pertaining to the intermolecular vibrational energies of the HCl trimer that could be directly compared to our 12D results are very limited. The only experimental information available comes from Ref. 43, which reports two intermolecular vibrational transitions, at 229.9 and 239.3 cm^{-1}, measured in a Ne matrix isolation experiment. They were assigned to the out-of-plane symmetric bend and in-plane asymmetric bend, respectively, but the authors of Ref. 43 do not exclude the reverse assignment either.

These measured values are in reasonable agreement with our computed 12D values of 225.02 cm^{-1} for ν_{osb} and 228.55 cm^{-1} for ν_{iab}. However, it is important to note that transition frequencies measured in the Ne matrix can be lower than the gas-phase values by several cm^{-1} (e.g., see Table IX of Ref. 35 for the HF trimer).

2. Intramolecular vibrations

Table VIII presents the energies (in cm^{-1}) of the $v = 1, 2$ HCl-stretching states of the HCl trimer computed in 12D, for intermolecular vibrational modes in the ground state. Table VIII also presents the corresponding intramolecular vibrational energies from the reduced-dimension 3D calculations, obtained for both $V_{intra}^{(eq)}$ and $V_{intra}^{(avg)}$. The comparison between the 12D and 3D intramolecular eigenenergies is informative about the strength of the coupling between the intramolecular and intermolecular vibrations of the trimer, with a caveat discussed below. As expected, using $V_{intra}^{(avg)}$ in the 3D calculations yields energies in a much better agreement with those from the 12D calculations than when $V_{intra}^{(eq)}$ is utilized. In fact, the 3D values of the ν_{sym}^{HCl} and ν_{asym}^{HCl} fundamentals obtained with $V_{intra}^{(avg)}$ are only ≈7 cm^{-1} (less than 0.3%) lower than the respective 12D values. For the higher excited intramolecular states, overtone and combination states, presented in Table VIII, the difference between their 12D and 3D $V_{intra}^{(avg)}$ values is less than 15 cm^{-1} or ≈0.3% as well.

These results suggest very weak coupling between the excited intra- and inter-molecular vibrational modes of the HCl trimer. However, it should be remembered that in $\hat{H}_{intra}$, the potential $V_{intra}^{(avg)}$ is defined by the constants ($\bar{R}_k$ = 7.1 bohrs, $\bar{\phi}_k = 50°$ and $\bar{\theta}_k = 90°$) that are the expectation values associated with the intermolecular vibrational ground state of the 9D $\hat{H}_{inter}$. Hence, as pointed out in Ref. 35, the 3D V_{intra} is a "trimer-adapted" potential for the collective intramonomer vibrations of the trimer, which incorporates information from the sophisticated 9D calculations and not just a sum of three isolated-monomer potentials. For this reason, the eigenstates of $\hat{H}_{intra}$ are anticipated to capture, to a significant degree, the effect of the intermonomer interactions on the intramonomer vibrations, i.e., the inter–intra coupling, in the trimer. Excellent agreement for the intramolecular vibrational energies presented in Table VIII from the 3D and 12D calculations bears out this expectation.

As mentioned earlier, hydrogen-bond formation results in shifts in the frequencies of the intramolecular vibrations of the monomers in a molecular complex away from the vibrational frequencies of the isolated monomers. We accurately characterized such vibrational frequency shifts in the past couple of years for several triatom–diatom molecular complexes, H_2O/D_2O–CO,[15] HDO-CO,[26] and HCl–H_2O,[27] by means of full-dimensional (9D) quantum calculations of their inter- and intra-molecular vibrations. Most recently, these rigorous quantum calculations, in 12D, were extended to the vibrational frequency shifts for the HF trimer.[35]

The 12D results presented in Table VIII allow us to calculate the frequency shifts for the HCl trimer. On the PES employed, when the three monomers are at a large separation, the $v = 1$ vibrational level of the isolated HCl is at 2886.19 cm^{-1} (the measured value is 2885.9777 cm^{-1}). This combined with the results presented in Table VIII gives for the trimer vibrational states ν_{sym}^{HCl} and ν_{asym}^{HCl}, the frequency shifts (redshifts) of −67.02 and −50.31 cm^{-1}, respectively. The redshift calculated for ν_{asym}^{HCl} is somewhat smaller than the measured shift of −76.20 cm^{-1},[39] implying that the current PES slightly underestimates the strength of the hydrogen bonding in the HCl trimer. In the case of the HF trimer, the redshifts calculated by us[35] for the ν_{sym}^{HF} and ν_{asym}^{HF} fundamentals are −280.43 and −216.78 cm^{-1}, respectively. Clearly, they are much larger than their counterparts in the HCl trimer, reflecting the much stronger hydrogen bonding in the HF trimer than in HCl trimer.

It is instructive to compare the intramolecular vibrational energies of HCl trimer obtained in our 12D calculations to those from the reduced-dimension LMon–Hückel and three-mode coupling models in Ref. 46 employing the same PES, neither of which includes the coupling between the intra- and inter-molecular modes of the trimer. The three-mode model[46] is essentially equivalent to our 3D intramolecular vibrational treatment in Sec. III A 4, with $V_{intra}^{(eq)}$, which also lacks the intra/inter mode coupling. Not surprisingly, in this work, both approaches yield virtually the same energies for ν_{asym}^{HCl}, 2814 cm^{-1} (3-mode[46]) and 2813 cm^{-1} (Table VIII).

In the LMon–Hückel treatment,[46] the local anharmonic HCl stretching frequencies are computed using a 1D potential cut along each monomer's local HCl stretching mode. They are then split into the desired 1:2 degeneracy pattern using a Hückel matrix, where the splitting is set to be equal to the splitting of the harmonic frequencies. This LMon–Hückel model gives 2815 cm^{-1} for ν_{asym}^{HCl}, nearly identical to that of the three-mode coupling model.

Thus, all three 3D intramolecular treatments give very similar energies for ν_{asym}^{HCl}, 2813–2815 cm^{-1}, which is in good agreement with the measured value[41] of 2810 cm^{-1}. In fact, they agree with the experiment better than the energy of ν_{asym}^{HCl} from the fully coupled 12D calculations, 2836 cm^{-1} (Table VIII). However, the 3D treatments of the intramolecular monomer vibrations do not include coupling to the intermolecular vibrations of the trimer, which is done rigorously by the 12D calculations. Therefore, one is led to conclude that the better agreement of the reduced-dimension calculations with an experimental value in this case is fortuitous, caused by the cancellation of errors arising from the approximations in bound-state methodology and the residual inaccuracies of the PES employed.

3. Coupling between the inter- and intra-molecular vibrational modes of the HCl trimer

One measure of the strength of the coupling between the inter- and intra-molecular vibrational modes of the trimer is the degree to which the intermolecular excitation energies vary in different intramolecular excitation manifolds. In order to quantify this inter/intra coupling, Table IX presents the energies of the fundamentals of the intermolecular stretching and bending modes of the trimer for both the intramolecular ground state and the excited $v = 1$ ν_{sym}^{HCl} and ν_{asym}^{HCl} intramolecular vibrational manifolds, from 12D calculations. They are obtained by taking the energies of the vibrations involving the combined inter- and intra-molecular excitations and subtracting from them the corresponding pure intramolecular vibrational energy. Similar to what was found for the HF

TABLE IX. Intermolecular excitation energies (in cm^{-1}) in the ground state and the ν_{sym}^{HCl} and ν_{asym}^{HCl} intramolecular manifolds of the HCl trimer, obtained from 12D calculations.

Excitation	gs	ν_{sym}^{HCl}[a]	ν_{asym}^{HCl}[b]
ν_{as}	75.94	79.47	(77.20, 78.17, 78.18)
ν_{ss}	93.29	97.44	95.29
ν_{oab}	169.22	178.81	(173.69, 176.40, 177.85)
ν_{osb}	225.02	237.77	233.15
ν_{iab}	228.55	238.4[c]	(233.63, 235.31, 237.70)
ν_{isb}	374.3[d]	387.63	383.57

[a]Energies relative to the intramolecular excitation energy of 2819.17 cm^{-1}.
[b]Energies relative to the intramolecular excitation energy of 2835.88 cm^{-1}.
[c]Average energy of the two candidate states, 237.93 and 238.77 cm^{-1}.
[d]Average energy of the two candidate states, 373.96 and 374.72 cm^{-1}.

trimer,[35] the excitation energies of all intermolecular modes considered are higher in both $v = 1$ HCl-stretch excited intramolecular manifolds than in the ground intramolecular vibrational state. Moreover, they are slightly higher for ν_{sym}^{HCl} excitation than for ν_{asym}^{HCl}. The differences between the intermolecular excitation energies in the $v = 1$ and $v = 0$ intramolecular excitation manifolds are much smaller in magnitude for the HCl trimer than for the HF trimer, but only slightly smaller in relative terms when compared to the respective intermolecular vibrational energies. By this measure, the magnitude of inter–intra coupling is comparable in HCl and HF trimers.

One more piece of evidence for the coupling between the intra- and inter-molecular vibrations of the HCl trimer is provided by the two entries at the bottom of Table VI. They show that, surprisingly, excitation of the intramolecular ν_{sym}^{HCl} and ν_{asym}^{HCl} fundamentals results in the appreciable shortening of the vibrationally averaged distance between HCl monomers, from 7.040 bohrs in the ground state to 7.011 bohrs for the ν_{sym}^{HCl} fundamental and 7.022 bohrs for the ν_{asym}^{HCl}. Similar effects were observed for the HF trimer.[35] Evidently, the coupling between intra- and inter-molecular modes of the HCl (and HF) trimer manifests in the changes of both its vibrational energy level structure and geometric features due to the intramolecular vibrational excitations, and the observed changes suggest that the H-bonding becomes stronger in the $v = 1$ intramolecular manifold.

4. Cooperative hydrogen bonding—The role of the three-body interaction

A distinctive aspect of molecular trimers is that these are the smallest systems in which nonadditive many-body (three-body in this case) interactions are present, leading to cooperative bonding. One way to assess the significance of the three-body interactions in a molecular trimer is by performing bound-state calculations for a trimer on a pairwise additive two-body PES that does not include the three-body interactions and compare the resulting structural and spectroscopic properties to those obtained for the 2 + 3-body PES in which the three-body interactions are present. This route is feasible in the present study, because the 12D PES of the HCl trimer that we employ is expressed as a sum of one-, two-, and three-body terms. Table X presents different quantities calculated for the HCl trimer on the full 2 + 3-body PES and on the two-body PES. Since the three-body interaction is always attractive, its omission weakens the hydrogen bonds between the monomers and increases the intermonomer separations. All the differences between the 2 + 3-body and two-body results presented in Table X can be understood qualitatively in terms of these two features, and the 12D calculations can quantify them.

If the three-body interaction is excluded, on the two-body trimer PES, the energy of the global minimum (D_e) decreases in absolute value by 285 cm^{-1}, relative to that for the 2 + 3-body

TABLE X. Various quantities computed in 12D on the full 2 + 3-body PES and on the two-body PES. Energies are in cm^{-1}, distances are in bohrs, and angles are in degrees. Here, q_e ($q = r, R, \theta, \phi$) denotes the internal coordinates in the equilibrium structure, while $\langle q \rangle (\Delta q)$ corresponds to the ground state. $\nu^{HCl} = 2886.19$ cm^{-1} is the stretching fundamental frequency of the isolated HCl, computed on the PES employed.

	2 + 3-body PES	2-Body PES		2 + 3-body PES	2-Body PES
D_e	2335.52	2050.14	ν_{sym}^{HCl}	2819.17	2831.41
D_0	1526.83	1331.25	ν_{asym}^{HCl}	2835.88	2843.80
r_e	2.4245	2.4194	$\nu_{sym}^{HCl} - \nu^{HCl}$	−67.02	−54.78
R_e	6.9196	7.0356	$\nu_{asym}^{HCl} - \nu^{HCl}$	−50.31	−42.39
ϕ_e	47.6534	48.52	ν_{as}	75.94	62.85
θ_e	90.00	90.00	ν_{ss}	93.29	82.77
$\langle r \rangle (\Delta r)$	2.452 (0.147)	2.450 (0.146)	ν_{oab}[a]	169.44	140.19
$\langle R \rangle (\Delta R)$	7.040 (0.197)	7.158 (0.212)	ν_{osb}[b]	225.55	191.84
			ν_{iab}	228.55	187.29
			ν_{isb}	374.3[c]	330.62

[a]From 9D calculation with $\bar{r} = \bar{r}_0$.
[b]From 9D calculation with $\bar{r} = \bar{r}_0$.
[c]Average energy of the two candidate states, 373.96 and 374.72 cm^{-1}.

PES. In addition, the equilibrium and also the vibrationally averaged (ground state) intermonomer distances, R_e and $\langle R \rangle$, respectively, are larger on the two-body PES than on the 2 + 3-body PES.

Regarding the trimer energetics, the two-body 12D binding energy D_0 of the HCl trimer with respect to the complete dissociation channel $(HCl)_3$ (g.s.) → 3 HCl (g.s.), 1331.25 cm^{-1}, is smaller by 196 cm^{-1} than the D_0 for the same channel on the 2 + 3-body PES, 1526.83 cm^{-1}.

The 12D binding energy D_0 of the HCl trimer with respect to the $(HCl)_3$ (g.s.) → $(HCl)_2$ (g.s.) + HCl (g.s.) channel can also be readily calculated for both the 2 + 3-body and two-body PESs. As mentioned above, on the 2 + 3-body PES, the 12D binding energy of the HCl trimer in the ground state relative to that of the three HCl (g.s.) monomers is 1526.83 cm^{-1}, compared to 1331.25 cm^{-1} on the two-body PES. On the other hand, the 6D binding energy of the isolated HCl dimer on the ES1-EL PES[10] is 425.26 cm^{-1}. Therefore, on the 2 + 3-body PES, the binding energy of the HCl trimer relative to $(HCl)_2$ (g.s.) + HCl (g.s.) is 1526.83–425.26 = 1101.57 cm^{-1}. On the two-body PES, for the same channel, the D_0 is 1331.25–425.26 = 905.99 cm^{-1}.

For both $(HCl)_3$ dissociation channels above, our 12D D_0 values calculated on the 2 + 3 body PES are in excellent agreement with those from the DMC calculations on the same PES and also agree well with the experimental results,[42] unlike the corresponding 12D results obtained for the two-body PES in this work.

It is evident from Table X that the three-body term has a large effect on the vibrational transition energies, as well as intra- and inter-molecular energies. On the two-body PES, with the three-body term excluded, the energies of all intermolecular vibrational fundamentals are significantly lower, by more than 40 cm^{-1} for the in-plane bend modes, than those of their counterparts on the 2 + 3-body PES.

As mentioned in Sec. III B 1, the only experimental information regarding the intermolecular vibrations of $(HCl)_3$ comes from Ref. 43. Reported there are two intermolecular vibrational transitions, at 229.9 and 239.3 cm^{-1}, measured in a Ne matrix isolation experiment and tentatively assigned to the out-of-plane symmetric bend and in-plane asymmetric bend, respectively (although the authors of Ref. 43 do not exclude the possibility of a reverse assignment). These measured values are in much better agreement with the 12D values computed on the 2 + 3-body PES, 225.02 cm^{-1} for ν_{osb} and 228.55 cm^{-1} for ν_{iab}, than with those for the two-body PES, 191.84 and 187.29 cm^{-1}, respectively.

The energies of the two HCl-stretch fundamentals of the trimer, ν_{sym}^{HCl} and ν_{asym}^{HCl}, are lower on the 2 + 3-body PES than on the two-body PES. This is due to the stronger hydrogen bonding and larger frequency redshifts on the 2 + 3-body PES in comparison with those for the two-body PES. The redshift calculated for ν_{asym}^{HCl} on the 2 + 3-body PES, −50.31 cm^{-1}, is closer to the measured[39] redshift of −76.20 cm^{-1} than the value obtained for the two-body PES, −42.39 cm^{-1}.

One can conclude that the three-body interactions have a strong impact on the energetics and the vibrations of the HCl trimer, and that their inclusion is essential for achieving good agreement with the experiment regarding the dissociation energies of the trimer and the energies of its intra- and inter-molecular vibrational states.

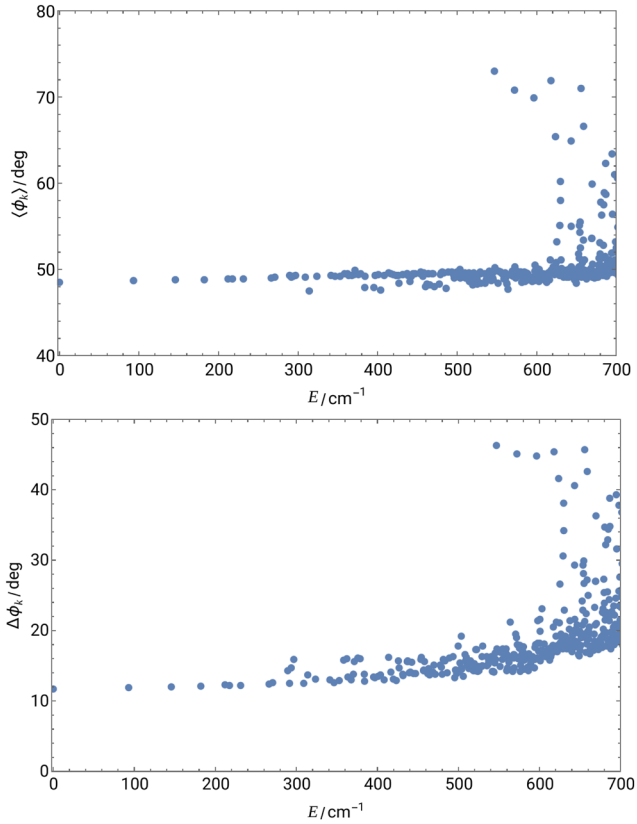

FIG. 2. $\langle\phi\rangle$ (top) and $\Delta\phi$ (bottom) for the A_1'-symmetry eigenstates of the 9D intermolecular Hamiltonian with $\tilde{r}$ = 2.452 bohrs. Outlier points with large $\langle\phi\rangle$ and large $\Delta\phi$ are states (partially) localized in the Z secondary minimum.

C. Vibrational states localized in the secondary minima

Vibrational states localized in the secondary minima of the PES are expected to play an important role in the predissociation mechanism of the HCl trimer, as suggested by the experimental[41,42] and computational[42] evidence. If the intramolecular asymmetric stretch is excited, its vibrational energy is first transferred to the intermolecular modes, followed by breaking of a hydrogen bond, which results in an open-chain configuration of the trimer. Next, the open-chain HCl trimer dissociates via two channels, $(HCl)_3$ → 3HCl or $(HCl)_3$ → HCl + $(HCl)_2$, the latter being the dominant channel according to Ref. 42. Motivated by this, we look for vibrational states corresponding to an open-chain configuration, i.e., states (partially) localized in the Z or Y secondary minimum (see Table I). We are able to identify some states localized in the Z secondary minimum based on the $\langle\phi_k\rangle(\Delta\phi_k)$ values and the 2D reduced probability density[34] (RPD) plots along ϕ_1 and ϕ_2, as shown in Fig. 2. For low-lying states localized in the global minimum, $\langle\phi_k\rangle \approx 49^\circ$ and $\Delta\phi_k$ is typically between 12° and 18°, but there are some outlier states at higher

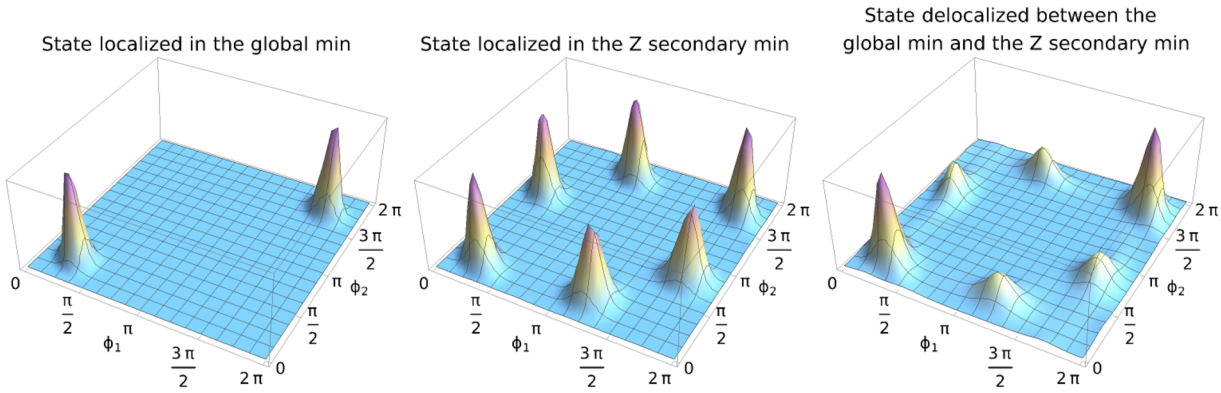

FIG. 3. 2D reduced probability density plot (RPD) along ϕ_1 and ϕ_2 for three representative states of the HCl trimer: one localized in the global minimum, the other in the Z secondary minimum, and the third delocalized between the global minimum and the Z secondary minimum. The RPD plots shown are obtained from 6D bend eigenstates. For additional details, see the text.

energies for which $\langle\phi_k\rangle$ is as large as 70° and $\Delta\phi_k$ can be 40°. Such outlier states are found among both 6D bending eigenstates and 9D intermolecular eigenstates.

These states are further investigated by calculating the (ϕ_1, ϕ_2) RPD plot for the 6D bending states. Let us assume that the molecule is localized close to a structure with non-equal $\phi_{k,0}$ values, that is, $\phi_{1,0} \neq \phi_{2,0} \neq \phi_{3,0}$. In this case, the (ϕ_1, ϕ_2) RPD plot shows six peaks due to permutation of the HCl monomers. The positions of the peaks are $(\phi_1, \phi_2) = (\phi_{1,0}, \phi_{2,0}), (\phi_{2,0}, \phi_{3,0})$ and $(\phi_{3,0}, \phi_{1,0})$ for even permutations and $(\phi_1, \phi_2) = (2\pi - \phi_{2,0}, 2\pi - \phi_{1,0}), (2\pi - \phi_{3,0}, 2\pi - \phi_{2,0})$ and $(2\pi - \phi_{1,0}, 2\pi - \phi_{3,0})$ for odd permutations. If $\phi_{k,0} = \phi_{j,0}$ for $j \neq k$, then certain peaks coincide. For example, for states localized in the global minimum, all $\phi_{k,0}$ are equal so there will be only two peaks, for $(\phi_1, \phi_2) = (49°, 49°)$ and (311°, 311°) (see Fig. 3), corresponding to the clockwise and counter-clockwise versions, respectively. The (ϕ_1, ϕ_2) RPD plots of most states look like the example in the left panel shown in Fig. 3 because they are localized in the global minimum. The (ϕ_1, ϕ_2) RPD plot of the outlier states mentioned before is characterized by six peaks (in the middle panel shown in Fig. 3), and the peak positions agree with the ϕ_k values of the Z secondary minimum (see Table I), meaning that these states are (mostly) localized in the Z secondary minimum. We also find many states delocalized between the global minimum and the Z secondary minimum. For these states, the (ϕ_1, ϕ_2) RPD plots also exhibit six peaks, but the peaks corresponding to (50°, 50°) and (310°, 310°) are larger than the other four because these are present for states localized in the global minimum and also for states localized in the Z secondary minimum (in the right panel shown in Fig. 3).

Table XI presents the lowest-energy intermolecular vibrational states localized in the Z secondary minimum. These nearly degenerate states most likely belong to the sixfold split ground state of the Z secondary minimum (note that there are six equivalent Z minima on the PES). Their energies are obtained from the 9D rigid-monomer intermolecular calculation with $\bar{r} = 2.452$ bohrs and are assigned to the Z minimum based on the $\langle\phi_k\rangle \approx$ and $\Delta\phi_k$ values. It should be noted that these values are not as accurate as those for the states in the global minimum reported in this paper because the PES employed[46] was developed to accurately describe the region around the global minimum and it is less reliable around the secondary minima,[49] and for this reason, we have not performed extensive convergence tests for these states. A more detailed exploration of them may be warranted in the future once a detailed and reliable trimer PES in the neighborhood of the local minima is available.

TABLE XI. Six-fold split intermolecular vibrational ground state of the Z secondary minimum from the 9D rigid-monomer calculations with $\bar{r} = 2.452$ bohrs. The ΔE energies, measured from the ZPE corresponding to the global minimum, are in cm^{-1}.

ΔE	Irrep	$\langle\phi_1\rangle(\Delta\phi_1)$	$\langle\phi_2\rangle(\Delta\phi_2)$	$\langle\phi_3\rangle(\Delta\phi_3)$	$(\Delta\theta_1, \Delta\theta_3, \Delta\theta_3)$
546.87	A_1'	73.0 (46.3)	73.2 (46.4)	73.2 (46.4)	(18.8, 18.3, 18.3)
546.84	E_a'	84.7 (48.6)	78.5 (48.0)	78.5 (48.0)	(20.2, 17.7, 17.7)
546.84	E_b'	61.9 (41.2)	68.6 (44.5)	68.6 (44.5)	(17.4, 18.8, 18.8)
546.94	E_a'	60.2 (40.1)	70.2 (45.3)	70.2 (45.3)	(17.3, 18.0, 18.0)
546.94	E_b'	86.7 (48.6)	77.6 (47.9)	77.6 (47.9)	(20.2, 18.3, 18.3)
546.96	A_2'	73.0 (46.2)	73.3 (46.4)	73.3 (46.4)	(18.7, 18.2, 18.2)

IV. CONCLUSIONS

In this paper, we present the first rigorous full-dimensional (12D) quantum calculations of the fully coupled intra- and intermolecular vibrational states of the HCl trimer. We recently introduced the computational methodology employed in these calculations in Ref. 35, where it was implemented for the 12D calculations of the HF-stretch excited vibrational states of the HF trimer. The calculations in this work utilize the 12D PES of Mancini and Bowman.[46]

When HCl monomers are in their ground intramolecular vibrational states, the energies of the low-lying intermolecular vibrational states of the trimer considered, obtained by the 12D (flexible-monomer) calculations, agree to within 2 cm^{-1} with those from the

rigid-monomer 9D calculations of the intermolecular eigenstates. However, it should be noted that the fixed HCl bond length used in the 9D calculations corresponds to the (trimer-adapted) expectation value for the ground state of the trimer from the 3D intramolecular vibrational calculation, which partially includes the effect of the trimer hydrogen bonding.

This paper also reports the 12D energies of the $v = 1, 2$ HCl-stretch excited intramolecular vibrational states, together with the intermolecular vibrational states in the excited $v = 1$ $\nu_{\rm sym}^{\rm HCl}$ and $\nu_{\rm asym}^{\rm HCl}$ intramolecular vibrational manifolds. Comparison of the 12D results with those from the 3D intramolecular vibrational calculations shows that the 3D values of $\nu_{\rm sym}^{\rm HCl}$ and $\nu_{\rm asym}^{\rm HCl}$ fundamentals are only $\approx$7 cm^{-1} (less than 0.3%) lower than the respective 12D values. This can be taken to imply a weak coupling between the excited intra- and inter-molecular vibrational modes of the HCl trimer. However, it should be remembered that the potential employed in the 3D intramolecular vibrational calculations is trimer-adaped, i.e., it incorporates key information from the sophisticated 9D intermolecular vibrational calculations. Therefore, it includes, to a significant degree, the effect of the intermonomer interactions on the intramonomer vibrations.

One measure of the strength of the coupling between the inter- and intra-molecular vibrational modes of the trimer is how the intermolecular vibrational energies change upon the excitation of the intramolecular vibrational modes. Our 12D calculations show that the excitation energies of all intermolecular modes considered are higher in both $v = 1$ HCl-stretch excited intramolecular manifolds, by 4–13 cm^{-1}, than in the ground intramolecular vibrational state. The same effect was found for the HF trimer.[35]

Our 12D quantum calculations yield for the HCl trimer vibrational states, $\nu_{\rm sym}^{\rm HCl}$ and $\nu_{\rm asym}^{\rm HCl}$, the frequency shifts (redshifts) of −67.02 and −50.31 cm^{-1}, respectively. The latter is somewhat smaller than the measured redshift of −76.20 cm^{-1}.[39] While appreciable, these $(HCl)_3$ redshifts are considerably smaller than those calculated by us in 12D for the $\nu_{\rm sym}^{\rm HF}$ and $\nu_{\rm asym}^{\rm HF}$ fundamentals of the HF trimer,[35] −280.43 and −216.78 cm^{-1}, respectively. Clearly, this is the result of the much stronger hydrogen bonding in the HF trimer than in the HCl trimer.

Molecular trimers provide a unique opportunity for quantifying the importance of the three-body interactions. In this work, we do it by comparing the results of the 12D calculations for the full 2 + 3-body PES[46] to those computed on the purely two-body PES obtained by removing the three-body term from the original PES. This comparison reveals that the absence of the three-body interaction affects strongly the energetics and the vibrational energies of the HCl trimer. Thus, the 12D binding energies D_0 of the HCl trimer with respect to the dissociation channels, $(HCl)_3$ (g.s.) → 3 HCl (g.s.) and $(HCl)_3$ (g.s.) → $(HCl)_2$ (g.s.) + HCl (g.s.), are about 200 cm^{-1} higher on the 2 + 3 body PES than on the two-body PES. In addition, the 2 + 3-body D_0 values agree much better with the experimental results[46] than the corresponding 12D results obtained for the two-body PES in this work.

The three-body term, or its absence, also has a large effect on the intra- and inter-molecular vibrational energies of the trimer. Thus, on the two-body PES, with the three-body term excluded, the energies of all intermolecular vibrational fundamentals are significantly lower, by more than 40 cm^{-1} for the in-plane bend modes, than those of their counterparts on the 2 + 3-body PES. Importantly, the energies of the $\nu_{\rm osb}$ and $\nu_{\rm iab}$ intermolecular fundamentals calculated in 12D on the 2 + 3-body PES agree much better with the results of the measurements for $(HCl)_3$ in a Ne matrix[43] than the values computed on the two-body PES. For the two HCl-stretch fundamentals of the trimer, $\nu_{\rm sym}^{\rm HCl}$ and $\nu_{\rm asym}^{\rm HCl}$, the energies calculated in 12D are lower on the 2 + 3-body PES than on the two-body PES due to stronger hydrogen bonding and larger frequency redshifts on the former PES.

The conclusion is that the three-body interactions strongly affect the energetics and the vibrations of the HCl trimer. Their inclusion is essential for an accurate description of the trimer properties and for achieving good agreement with the experiment.

Finally, low-energy vibrational states localized in a secondary minimum are identified, based on the expectation values and the rms deviations of suitably chosen coordinates and the RPD plots along them.

The 12D calculations for the HCl trimer in this paper, together with those in 12D for the HF trimer in Ref. 35, demonstrate the maturity of the methodology for rigorous, full-dimensional quantum calculations of the coupled intra- and inter-molecular vibrational states of noncovalently bound trimers of flexible diatomic molecules. It is our hope that these advances will motivate further experimental studies of these and other molecular trimers, for which scant spectroscopic data are currently available. Work is in progress in our group on extending this treatment to the 12D quantum calculations of the intermolecular vibration–rotation-tunneling states of the H_2O trimer in the rigid-monomer approximation.

SUPPLEMENTARY MATERIAL

See the supplementary material for the convergence tests and additional results for the eigenstates of the 3D $\hat{H}_F$, 6D $\hat{H}_B$, 9D $\hat{H}_{\rm inter}$, 3D $\hat{H}_{\rm intra}$, and 12D $\hat{H}$.

ACKNOWLEDGMENTS

We thank Professor Joel Bowman and Dr. Chen Qu for generously providing us with the code to compute the 12D potential energy surface of the HCl trimer. I.S. acknowledges the postdoctoral fellowship from the Simons Foundation through the Simons Center for Computational Physical Chemistry at NYU. I.S., Z.B., and P.M.F. also acknowledge the Simons Foundation for the computational resources acquired with its support that were used in this research. Z.B. and P.M.F. acknowledge the National Science Foundation for its partial support of this research through the Grant Nos. CHE-2054616 and CHE-2054604, respectively. P.M.F. thanks Professor Daniel Neuhauser for his support.

AUTHOR DECLARATIONS

Conflict of Interest

The authors have no conflicts to disclose.

Author Contributions

Irén Simkó: Conceptualization (equal); Data curation (equal); Formal analysis (equal); Investigation (equal); Methodology (equal); Software (equal); Validation (equal); Visualization (equal); Writing – original draft (equal); Writing – review & editing (equal). **Peter M. Felker**: Conceptualization (equal); Data curation (equal); Formal analysis (equal); Funding acquisition (equal); Investigation (equal); Methodology (equal); Project administration (equal); Resources (equal); Software (equal); Supervision (equal); Validation (equal); Visualization (equal); Writing – original draft (equal); Writing – review & editing (equal). **Zlatko Bačić**: Conceptualization (equal); Data curation (equal); Formal analysis (equal); Funding acquisition (equal); Investigation (equal); Methodology (equal); Project administration (equal); Resources (equal); Software (equal); Supervision (equal); Validation (equal); Visualization (equal); Writing – original draft (equal); Writing – review & editing (equal).

DATA AVAILABILITY

The data that support the findings of this study are available within the article and its supplementary material.

REFERENCES

[1] Z. Bačić and R. E. Miller, "Molecular clusters: Structure and dynamics of weakly bound systems," J. Phys. Chem. **100**, 12945 (1996).

[2] P. E. S. Wormer and A. van der Avoird, "Intermolecular potentials, internal motions, and spectra of van der Waals and hydrogen-bonded complexes," Chem. Rev. **100**, 4109 (2000).

[3] T. Carrington, Jr. and X.-G. Wang, "Computing ro-vibrational spectra of van der Waals molecules," Wiley Interdiscip. Rev.: Comput. Mol. Sci. **1**, 952 (2011).

[4] A. van der Avoird, "Vibration-rotation-tunneling levels and spectra of Van der Waals molecules," in *Vibrational Dynamics of Molecules*, edited by J. M. Bowman (World Scientific, Singapore, 2022), p. 194.

[5] E. Mátyus, A. Martín Santa Daria, and G. Avila, "Exact quantum dynamics developments for floppy molecular systems and complexes," Chem. Commun. **59**, 366 (2023).

[6] D. H. Zhang, Q. Wu, J. Z. H. Zhang, M. von Dirke, and Z. Bačić, "Exact full-dimensional bound state calculations for $(HF)_2$, $(DF)_2$, and HFDF," J. Chem. Phys. **102**, 2315 (1995).

[7] Q. Wu, D. H. Zhang, and J. Z. H. Zhang, "6D quantum calculation of energy levels of HF stretching excited $(HF)_2$," J. Chem. Phys. **103**, 2548 (1995).

[8] Z. Bačić and Y. Qiu, "Vibration-rotation-tunneling dynamics of $(HF)_2$ and $(HCl)_2$ from full-dimensional quantum bound-state calculations," in *Advances in Molecular Vibrations and Collision Dynamics*, edited by J. M. Bowman and Z. Bačić (JAI Press, Inc., Stamford, 1998), Vol. 3, p. 183.

[9] Y. Qiu and Z. Bačić, "Exact six-dimensional quantum calculations of the rovibrational levels of $(HCl)_2$," J. Chem. Phys. **106**, 2158 (1997).

[10] Y. Qiu, J. Z. H. Zhang, and Z. Bačić, "Six-dimensional quantum calculations of vibration-rotation-tunneling levels of ν_1 and ν_2 HCl-stretching excited $(HCl)_2$," J. Chem. Phys. **108**, 4804 (1998).

[11] G. W. M. Vissers, G. C. Groenenboom, and A. van der Avoird, "Spectrum and vibrational predissociation of the HF dimer. I. Bound and quasibound states," J. Chem. Phys. **119**, 277 (2003).

[12] J. Huang, D. Yang, Y. Zhou, and D. Xie, "A new full-dimensional *ab initio* intermolecular potential energy surface and vibrational states for $(HF)_2$ and $(DF)_2$," J. Chem. Phys. **150**, 154302 (2019).

[13] X.-G. Wang and T. Carrington, "Using monomer vibrational wavefunctions to compute numerically exact (12D) rovibrational levels of water dimer," J. Chem. Phys. **148**, 074108 (2018).

[14] P. M. Felker and Z. Bačić, "Weakly bound molecular dimers: Intramolecular vibrational fundamentals, overtones, and tunneling splittings from full-dimensional quantum calculations using compact contracted bases of intramolecular and low-energy rigid-monomer intermolecular eigenstates," J. Chem. Phys. **151**, 024305 (2019).

[15] P. M. Felker and Z. Bačić, "H_2O–CO and D_2O–CO complexes: Intra- and intermolecular rovibrational states from full-dimensional and fully coupled quantum calculations," J. Chem. Phys. **153**, 074107 (2020).

[16] Z. Bačić and J. C. Light, "Highly excited vibrational levels of "floppy" triatomic molecules: A discrete variable representation-distributed Gaussian basis approach," J. Chem. Phys. **85**, 4594 (1986).

[17] Z. Bačić and J. C. Light, "Accurate localized and delocalized vibrational states of HCN/HNC," J. Chem. Phys. **86**, 3065 (1987).

[18] Z. Bačić, R. M. Whitnell, D. Brown, and J. C. Light, "Localized representations for large amplitude molecular vibrations," Comput. Phys. Commun. **51**, 35 (1988).

[19] Z. Bačić and J. C. Light, "Theoretical methods for rovibrational states of floppy molecules," Annu. Rev. Phys. Chem. **40**, 469 (1989).

[20] X.-G. Wang and T. Carrington, Jr., "New ideas for using contracted basis functions with a Lanczos eigensolver for computing vibrational spectra of molecules with four or more atoms," J. Chem. Phys. **117**, 6923 (2002).

[21] X.-G. Wang and T. Carrington, Jr., "A contracted basis-Lanczos calculation of vibrational levels of methane: Solving the Schrödinger equation in nine dimensions," J. Chem. Phys. **119**, 101 (2003).

[22] J. C. Tremblay and T. Carrington, "Calculating vibrational energies and wave functions of vinylidene using a contracted basis with a locally reorthogonalized coupled two-term Lanczos eigensolver," J. Chem. Phys. **125**, 094311 (2006).

[23] X.-G. Wang and T. Carrington, Jr., "Vibrational energy levels of CH_5^+," J. Chem. Phys. **129**, 234102 (2009).

[24] S. Zou, J. M. Bowman, and A. Brown, "Full-dimensionality quantum calculations of acetylene-vinylidene isomerization," J. Chem. Phys. **118**, 10012 (2003).

[25] D. Lauvergnat, P. M. Felker, Y. Scribano, D. M. Benoit, and Z. Bačić, "H_2, HD and D_2 in the small cage of structure II clathrate hydrate: Vibrational frequency shifts from fully coupled quantum six-dimensional calculations of the vibration-translation-rotation eigenstates," J. Chem. Phys. **150**, 154303 (2019).

[26] P. M. Felker and Z. Bačić, "HDO–CO complex: D-Bonded and H-bonded isomers and intra- and intermolecular rovibrational states from full-dimensional and fully coupled quantum calculations," J. Phys. Chem. A **125**, 980 (2021).

[27] Y. Liu, J. Li, P. M. Felker, and Z. Bačić, "HCl–H_2O dimer: An accurate full-dimensional potential energy surface and fully coupled quantum calculations of intra- and intermolecular vibrational states and frequency shifts," Phys. Chem. Chem. Phys. **23**, 7101 (2021).

[28] P. M. Felker, Y. Liu, J. Li, and Z. Bačić, "DCl–H_2O, HCl–D_2O, and DCl–D_2O dimers: Inter- and intramolecular vibrational states and frequency shifts from fully coupled quantum calculations on a full-dimensional neural network potential energy surface," J. Phys. Chem. A **125**, 6437 (2021).

[29] P. M. Felker and Z. Bačić, "Inter- and intramolecular rovibrational states of HCl–H_2O and DCl–H_2O dimers from full-dimensional and fully coupled quantum calculations," Chin. J. Chem. Phys. **34**, 728 (2021).

[30] P. M. Felker and Z. Bačić, "Benzene-H_2O and benzene-HDO: Fully coupled nine-dimensional quantum calculations of flexible H_2O/HDO intramolecular vibrational excitations and intermolecular states of the dimers, and their infrared and Raman spectra using compact bases," J. Chem. Phys. **152**, 124103 (2020).

[31] P. M. Felker and Z. Bačić, "Flexible water molecule in C_{60}: Intramolecular vibrational frequencies and translation-rotation eigenstates from fully coupled nine-dimensional quantum calculations with small basis sets," J. Chem. Phys. **152**, 014108 (2020).

[32] X.-G. Wang and T. Carrington, "Computing excited OH stretch states of water dimer in 12D using contracted intermolecular and intramolecular basis functions," J. Chem. Phys. **158**, 084107 (2023).

[33] P. M. Felker and Z. Bačić, "Noncovalently bound molecular complexes beyond diatom–diatom systems: Full-dimensional, fully coupled quantum calculations of rovibrational states," Phys. Chem. Chem. Phys. **24**, 24655 (2022).

[34]P. M. Felker and Z. Bačić, "Intermolecular vibrational states of HF trimer from rigorous nine-dimensional quantum calculations: Strong coupling between intermolecular bending and stretching vibrations and the importance of the three-body interactions," J. Chem. Phys. **157**, 194103 (2022).
[35]P. M. Felker and Z. Bačić, "HF trimer: 12D fully coupled quantum calculations of HF-stretch excited intramolecular and intermolecular vibrational states using contracted bases of intramolecular and intermolecular eigenstates," J. Chem. Phys. **158**(23), 234109 (2023).
[36]X.-G. Wang and T. Carrington, Jr., "An exact kinetic energy operator for $(HF)_3$ in terms of local polar and azimuthal angles," Can. J. Phys. **79**, 623 (2001).
[37]W. Klopper, M. Quack, and M. A. Suhm, "HF dimer: Empirically refined analytical potential energy and dipole hypersurfaces from *ab initio* calculations," J. Chem. Phys. **108**, 10096 (1998).
[38]M. Quack, J. Stohner, and M. A. Suhm, "Analytical three-body interaction potentials and hydrogen-bond dynamics of hydrogen fluoride aggregates, $(HF)_n$, $n \geq 3$," J. Mol. Struct. **599**, 381 (2001).
[39]J. Han, Z. Wang, A. L. McIntosh, R. R. Lucchese, and J. W. Bevan, "Investigation of the ground vibrational state structure of HCl trimer based on the resolved K, J substructure of the ν_5 vibrational band," J. Chem. Phys. **100**, 7101 (1994).
[40]M. Farnik, S. Davis, and D. J. Nesbitt, "High-resolution IR studies of hydrogen bonded clusters: Large amplitude dynamics in $(HCl)_n$," Faraday Discuss. **118**, 63 (2001).
[41]M. Fárník, D. J. Nesbitt, and D. J. Nesbitt, "Intramolecular energy transfer between oriented chromophores: High-resolution infrared spectroscopy of HCl trimer," J. Chem. Phys. **121**, 12386 (2004).
[42]J. S. Mancini, A. K. Samanta, J. M. Bowman, and H. Reisler, "Experiment and theory elucidate the multichannel predissociation dynamics of the HCl trimer: Breaking up is hard to do," J. Phys. Chem. A **118**, 8402 (2014).
[43]A. Engdahl and B. Nelander, "The far-infrared spectrum of the hydrogen chloride trimer: A matrix isolation study," J. Phys. Chem. **94**(25), 8777–8780 (1990).
[44]Z. Latajka and S. Scheiner, "Structure, energetics and vibrational spectra of dimers, trimers, and tetramers of HX (X = Cl, Br, I)," Chem. Phys. **216**(1–2), 37–52 (1997).
[45]J. S. Mancini and J. M. Bowman, "*On-the-fly ab intito* calculations of anharmonic vibrational frequencies: Local-monomer theory and application to HCl clusters," J. Chem. Phys. **139**, 164115 (2013).
[46]J. S. Mancini and J. M. Bowman, "A new many-body potential energy surface for HCl clusters and its application to anharmonic spectroscopy and vibration-vibration energy transfer in the HCl trimer," J. Phys. Chem. A **118**, 7367 (2014).
[47]J. A. Coxon and P. G. Hajigeorgiou, "The radial Hamiltonians for the $X^1\Sigma^+$ and $B^1\Sigma^+$ states of HCl," J. Mol. Spectrosc. **203**(1), 49–64 (2000).
[48]M. J. Elrod and R. J. Saykally, "Vibration-rotation-tunneling dynamics calculations for the four-dimensional $(HCl)_2$ system: A test of approximate models," J. Chem. Phys. **103**, 921 (1995).
[49]J. Bowman, private communication (2023).
[50]M. J. Bramley and T. Carrington, Jr., "Calculation of triatomic vibrational eigenstates: Product or contracted basis sets, Lanczos or conventional eigensolvers? What is the most efficient combination?," J. Chem. Phys. **101**, 8494 (1994).
[51]P. R. Bunker and P. Jensen, *Molecular Symmetry and Spectroscopy* (NRC Research Press, Ottawa, ON, 1998).
[52]H. Wei and T. Carrington, Jr., "The discrete variable representation of a triatomic Hamiltonian in bond length-bond angle coordinates," J. Chem. Phys. **97**, 3029 (1992).
[53]J. Echave and D. C. Clary, "Potential optimized discrete variable representation," Chem. Phys. Lett. **190**, 225 (1992).